LhARA/ITRF: six month progress report

C. Baker [1], J. Bamber [2], W. Bertsche [13,5], N. Bliss [3], E. Boella [4,5], N. Dover [6], R. Gray [7,5], E. Harris [2], M. Johnson [3,5], K. Kirkby [12,13,5], A. Kurup [6,8], K.R. Long [6,8], R. Mclauchlan [9], H. Owen [3,5], J.L. Parsons [10], J. Pasternak [6,8], T. Price [11], C. Whyte [7,5],

1. *Department of Physics, Faculty of Science and Engineering, Swansea University, Singleton Park, Swansea, SA2 8PP*
2. *Institute of Cancer Research, UK*
3. *UKRI-STFC Daresbury Laboratory, Sci-Tech Daresbury, Daresbury, Warrington, WA4 4AD, UK*
4. *Lancaster University, UK*
5. *Cockcroft Institute, Sci-Tech Daresbury, Daresbury, Warrington, WA4 4AD, UK*
6. *John Adams Institute, Imperial College London, Exhibition Road, London, SW7 2AZ, UK*
7. *Department of Physics, SUPA, University of Strathclyde, 16 Richmond Street, Glasgow, G1 1XQ, UK*
8. *UKRI-STFC Rutherford Appleton Laboratory, Didcot, OX11 0QX, UK*
9. *Imperial College NHS Healthcare Trust, The Bays, South Wharf Road, St Mary's Hospital, London W2 1NY, UK*
10. *Institute of Cancer and Genomic Sciences, University of Birmingham, Edgbaston, Birmingham, B15 2TT, UK*
11. *School of Physics and Astronomy, University of Birmingham, Edgbaston, Birmingham, B15 2TT, UK*
12. *Division of Cancer Sciences, Faculty of Biology, Medicine and Health, The University of Manchester, The Christie Proton Therapy Centre, The Cristie NHS Foundation Trust, Wimslow Rd, Manchester M20 4BX*
13. *Department of Physics and Astronomy, The University of Manchester, Oxford Rd, Manchester, M13 9PL, UK*

Contents

Introduction

The UKRI Infrastructure Fund is investing £2 million to kick-start research on the next generation of radiotherapy treatments for cancer through the development of the Ion Therapy Research Facility (ITRF).

The UK has a track record of innovation in cancer therapy. In the UK, a large number of patients are treated successfully using radiotherapy delivered using X-ray and/or proton beams. However, some tumours remain difficult to treat. There is evidence that heavier particles, such as helium and carbon ions, offer therapeutic advantages and may be of particular benefit in the of in these "hard to treat" tumours.

The ITRF brings together leading UK and international clinicians, scientists, engineers and industry. Together, they will develop the the ITRF, such that it will become a world leading radiobiology research facility that will underpin the transformation of the clinical practice of proton- and ion-beam radiotherapy. The two-year Preliminary Activity funded by the UKRI Infrastructure fund will allow the design and planning for the ITRF to be developed and position the UK and its international partners to pursue the development of the world-leading facility.

The ITRF will be served by the Laser-hybrid Accelerator for Radiobiological Applications (LhARA) through which the unique properties of a laser-driven proton and ion source will be harnessed to deliver intense beams with properties unattainable at any existing research or clinical ion-therapy facility in the world today. Ultimately, LhARA will provide a state-of-the-art testbed through which academic, clinical, laboratory, and industrial communities will develop new technologies for the delivery of radiation therapy that is more precise, flexible and cost effective.

The ITRF will be a unique, compact, single-site international research infrastructure delivering the world's first high-dose-rate ions from protons to carbon at energies sufficient for both *in-vitro* and *in-vivo* studies. The baseline technology is a laser-hybrid proton/ion source, as proposed by the existing, UK-led, international LhARA collaboration [1–5]. Alternative technology options, including a synchrotron, will be considered for comparison. To make efficient use of the resources available a collaboration agreement [6] with CERN has been established. The synchrotron comparison described in the report on Work Package 3 is scaled down in size from the CERN NIMMS [7] helium synchrotron design.

This report describes the progress and status of the project after 6 months of the 2 year ITRF Conceptual Design Report.

0   Work package 0: Project management

0.1   Documentation

ITRF project documents follow a document-naming and folder structure convention [8] and are stored on the ITRF SharePoint site [9]. Documents generated by the LhARA collaboration are stored on the LhARA wiki [1].

0.2   Project Reporting and Governance

The ITRF project delivery committee meets bi-monthly with membership; Principal Investigator, Project Manager, and Work Package Managers from 3 Work Packages:

Work package 1: LhARA;

Work package 2: ITRF Facilities and Costing; and

Work package 3: Conventional Technology.

Table 1: Sections and supporting documents forming the ITRF Project Management Plan.

1272-pa1-pm-pmp-0004-v1.5-roles-governance	1. Project Description
	2. Project Organisation
1272-pa1-pm-ppl-0001-v2.0 - ITRF schedule 2022-07-20 - full detail	3. Objectives & Deliverables
1272-pa1-pm-ppl-0004-v1.0 - ITRF CDR schedule 2023-03-09	4. Project Schedule
1272-pa1-pm-ppl-0005-v0.4 - ITRF milestones and deliverables 2023-03-09	5. Finance
1272-pa1-pm-fin-0002-v5.1-ITRF resource-breakdown-2022-04-05	6. Resources
1272-pa1-pm-fin-0004-v2.0-ITRF-spend-profile-2022-12-18	7. Procurement Plan
1272-pa1-pm-risk-0001-v0.4-ITRF-Risk	8. Risk Management
	9. Stakeholder Communication
1272-pa1-pm-rpt-0001-v3.0-project-reporting-schedule	10. Monitoring & Reporting
	11. Quality Plan
1272-pa1-pm-rpt-0003-v1.0-business-case	12. Benefits Realisation and Impact Plan
	13. SHE Plan
	14. Diversity Issues
	15. History

Project management is coordinated and recorded to enable the ITRF project manager to provide monthly project reports to the UKRI–STFC Project Review Committee and the UKRI Infrastructure Fund. Project reports cover: Progress; Finance; Risk; and Issues. The ITRF project has established a Project Board and and Advisory Committee that both meet at a frequency of once every 3–6 months. An ITRF project Roles and Responsibilities document has been established that covers the Project Sponsor, Project Manager, Project Team Members and Project Governance [10].

0.3 Quality Assurance

Project management is being conducted in accordance with the UKRI–STFC Project Management Framework and the STFC–Daresbury Laboratory ISO9001:2015 Quality Management System (QMS) [11]. Under the QMS processes and procedures, the ITRF project is subject to internal audits by STFC staff and external audits by the British Standards Institute (BSI) [12]. A Business Case [13] and Project Management Plan (PMP) [14] have been established. The Business Case details the potential benefits of the project and the PMP is the top level plan for the delivery of the project containing the subsections and related underpinning documents referenced in red text in table 1.

1 Work package 1: LhARA

The LhARA collaboration's long-term vision [15] is to transform the clinical practice of proton- and ion-beam therapy (IBT) by creating a fully automated, highly flexible system to harness the unique properties of laser-driven ion beams. Such a facility will be capable of delivering particle-beam therapy in completely new regimens by combining a variety of ion species from proton to carbon in a single treatment, exploiting ultra-high dose rates and novel temporal-, spatial- and spectral-fractionation schemes. The automated system will integrate patient, soft-tissue and dose-deposition imaging with real-time treatment planning to trigger the delivery of dose tailored to the individual patient in real time. The automated, triggerable system has the

potential to remove the requirement for a large gantry, thereby reducing the size and therefore the cost, of a clinical IBT facility and to increase patient throughput thereby reducing the cost of IBT per patient.

In October 2022, the UKRI Infrastructure Fund established a two-year "Ion Therapy Research Facility scoping project" [16]. This section reports on the progress made in the first six months in the development LhARA to serve the Ion Therapy Research Facility (ITRF). The objectives of the programme over the two-year Preliminary Activity are [4, 5]:

- Deliver the Conceptual Design Report for LhARA to serve the Ion Therapy Research Facility;
- Demonstrate the feasibility of the laser-driven creation of the requisite proton and ion flux through simulation and measurement;
- Create the detailed specification of a second Gabor-lens prototype through a programme of experiment, simulation, and design;
- Experimentally prove the principle of ion-acoustic dose-profile measurement; and
- Create a detailed specification for the *in-vitro* and *in-vivo* end stations through peer-group consultation, design and simulation.

1.1 Work package 1.1: Project Management

The LhARA project is managed through bi-weekly meetings of the Project Management Board (PMB) [17]. The PMB is attended by all Work Package Managers and is chaired by the LhARA Project Manager. Individual Work Packages [18–22] hold weekly or bi-weekly meetings to which the PMB and LhARA Executive Board [23] have standing invitations; attendance at these meetings allows the management team directly to engage with the R&D programme, monitor progress and stay abreast of developments.

The LhARA PMB provides monthly reports to the ITRF project manager. These reports include spend to date, highlights of progress and raise issues as they arise. The reports also include a forward look to the next months of planned activity. The monthly reports to the ITRF are condensed from monthly reports provided by the work package managers to the PMB. Progress to date has largely been as planned with no areas of significant concern.

A review of the LhARA collaboration's R&D proposal for the Preliminary Activity and Pre-construction Phase of the ITRF project was carried out in the autumn of 2022 by an international external expert review panel [24]. The collaboration's response [25] to the review panel's recommendations [26] was completed over the past six months.

The LhARA collaboration has started the process of refining and documenting its radiobiology objectives, ahead of an international expert review of these aspects of the LhARA programme. The review of the radiobiology programme will follow a process similar to the autumn 2022 review: a panel of internationally-recognised experts will be convened and charged with interrogating the LhARA collaboration's objectives. The outcomes of this radiobiology review will be recorded on the LhARA wiki [1] and in an expanded LhARA radiobiological-science baseline document.

Progress in the individual work packages is covered in the sections which follow and will not be repeated here. Highlights of the programme to date include:

- The first peer-group-consultation meeting [27] which attracted more than 50 participants drawn from the UK and overseas;
- Significant progress towards the revision of the low-energy transport line to provide additional flexibility in the beams that can be delivered;
- Detailed discussions on the ion source/capture interfaces. The discussions have led to an improved understanding of the challenges in this area;

- Good progress has been made towards the design of a proof-of-principle experiment to demonstrate the ion-acoustic dose-profile measurement technique; and
- 3D PIC simulations of the SCAPA configuration with an aluminium foil target have been carried out.

The third LhARA collaboration meeting was held in February 2023 at the University of Birmingham [28]. Discussion was robust with a full day's material presented to the collaboration. The date was chosen to coincide with the mid-term break in teaching, this led to the meeting occurring 6 weeks in advance of the preparation of the ITRF six monthly progress report. Future LhARA collaboration meetings will be scheduled to occur between university terms to maximise staff availability. Adjustment of the associated LhARA and ITRF review dates to occur shortly after the LhARA collaboration meetings will maximise efficiency as the progress presented and reviewed at the collaboration meetings can be prepared for submission to the ITRF review.

1.2   Work package 1.2: Laser-driven proton and ion source

1.2.1   Overview of Work Package 1.2 progress

Work Package 1.2 (WP1.2) is designed to develop and test the technology required for the laser-driven ion source for LhARA. To address this, WP1.2 has successfully developed an effective collaboration between all the major groups active in the development of laser-driven ion sources in the UK: University of Strathclyde; Queen's University Belfast; Lancaster University; Imperial College London; and the Central Laser Facility. The collaboration is working effectively, with regular meetings and cross-institute collaborative projects. The funding from the ITRF has enabled increased staff effort at the partner institutes and is allowing excellent progress to be made towards the WP1.2 milestones.

The first milestone, LhARA MS2.1, is to predict the optimised proton source for 100+ TW laser systems based on hydrodynamic and kinetic simulations. This milestone is due in September 2023 and we are on schedule to meet it. Preliminary simulations have been performed and analysed. Further simulations are investigating parametric optimisation of the proton source. Output from the preliminary simulations has already been shared with other work packages, particularly Work Package 6, to allow realistic beam parameters to be used in beamline modelling. More details will be given in subsection 1.2.2.

The second milestone, LhARA MS2.2, due in March 2024, is to perform the first SCAPA ion source simulations and experiments. We are on schedule to meet the milestone. During the first 6 months of the project, significant progress has been made in the design and development of the core experimental methodologies needed to realise the requirements of the proton and ion source for LhARA. At this initial developmental stage, much of the experimental work has been supported via complimentary access to SCAPA, funded from other sources, and competitive access to the Gemini laser at the Central Laser Facility (CLF). The first beam time dedicated to LhARA on SCAPA is now scheduled for July 2023. This short period of access will focus on producing initial parameter scans of the proton and ion beam properties (varying laser energy, pulse duration, spot size and plasma density scale-length). This experiment is an important first step to providing a data set to benchmark the simulation work and to support the development of high-repetition-rate targetry and diagnostics aimed specifically at the requirements of LhARA. This beam time will also be used to make measurements of target debris production in collaboration with the CLF and SciTech, who will provide support via their metrology capabilities. The focus of much of the experimental work in the past 6 months has been to prepare the ground for this first beam time. Details are shown below of developments over the past 6 months in key areas including: diagnostics, targetry and debris, data handling and control.

In addition, experiments have begun using the high repetition rate laser at Imperial College London to focus on targetry and technical issues related to high repetition rate. The experimental chamber has been prepared and the laser beamline is being readied to deliver the compressed femtosecond beam to target. The first ion
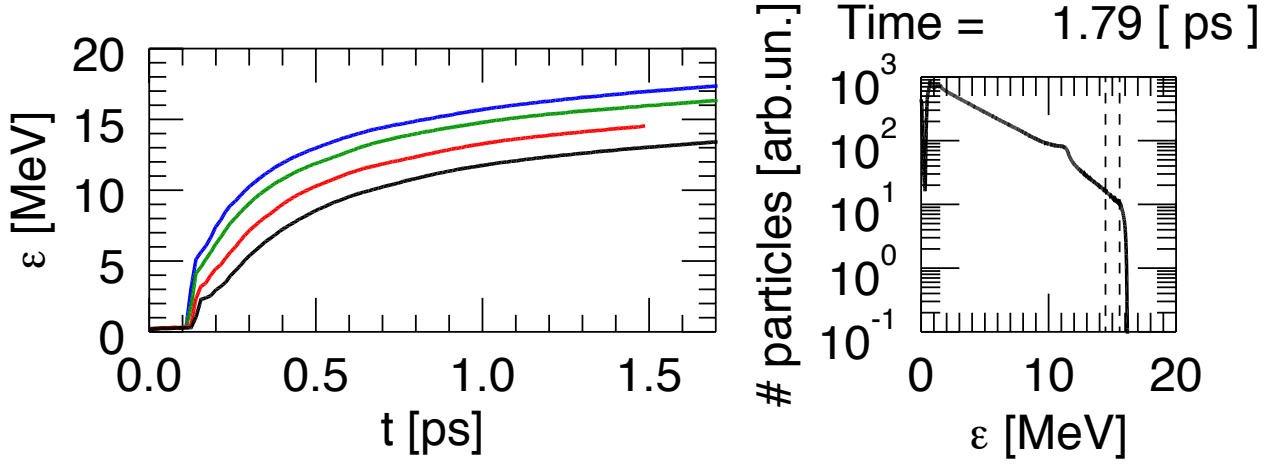
Figure 1: Evolution of the proton cutoff energy for different target thicknesses (left panel). Proton energy spectrum at saturation for a $2\,\mu$m thick Al target (right panel). The dashed lines indicate the range of energies of interest. These simulations consider a laser pulse with intensity $9 \times 10^{20}\,\mathrm{W/cm^2}$ and abrupt plasma-to-vacuum transition.

generation experiments are expected to begin in April 2023, with significant time available for LhARA related studies.

1.2.2 Update on Simulations

We have conducted realistic three-dimensional (3D) Particle-In-Cell (PIC) simulations exploring the interaction of the SCAPA Ti:sapphire laser (central laser wavelength $\lambda_0 = 800\,$nm) with aluminium foils. In these simulations, we performed parameter scans over laser intensity and target thickness. Laser intensities in the range $(8 - 10) \times 10^{20}\,\mathrm{W/cm^2}$, corresponding to normalised vector potentials $a_0 = 19.32 - 21.60$, were considered. The p-polarised pulses were focused on target to a spot size, w_0, of $1.5\,\mu$m and had a duration at FWHM of $25\,$fs. The target was modelled as a pre-formed plasma composed of Al^{3+} ions and electrons with density $70\,n_c \sim 10^{23}\,\mathrm{cm^{-3}}$ (here n_c is the critical density corresponding to the laser frequency). On the back of the target, a thin layer of H^+ ions was inserted to mimic contaminants naturally present on the back surface of solid targets.

Simulations using a range of target thicknesses revealed that, in the presence of optimal laser contrast and sharp plasma-to-vacuum transition, very thin targets (thicknesses $\leq 2\,\mu$m) must be used. Only with these very thin targets can proton spectra extending beyond $15\,$MeV be achieved (see the left panel of figure 1 which shows the maximum proton energy versus time for different target thicknesses in simulations employing a laser pulse with intensity on target $I = 9 \times 10^{20}\,\mathrm{W/cm^2}$). This finding requires a detailed evaluation of the laser temporal profile. In the presence of non-optimal contrasts and targets with these thicknesses, there is a concrete risk to disrupt the rear surface of the target by generating a plasma on this surface before the laser pulse reaches its maximum intensity on the front surface. This will deteriorate the performance of TNSA and lead to lower proton energies than those expected from simulation. We notice that, even under ideal conditions and with thin targets, at this intensity the proton cutoff energy will be $\sim 17\,$MeV. As a consequence, the range of energies in which we are interested ($14.5 - 15.5\,$MeV) will fall very close to the cutoff energy of the proton spectrum. This will make the whole scheme potentially susceptible to experimental fluctuations. It will also reduce the amount of charge available (see the right panel of figure 1 which shows the proton spectrum at saturation and
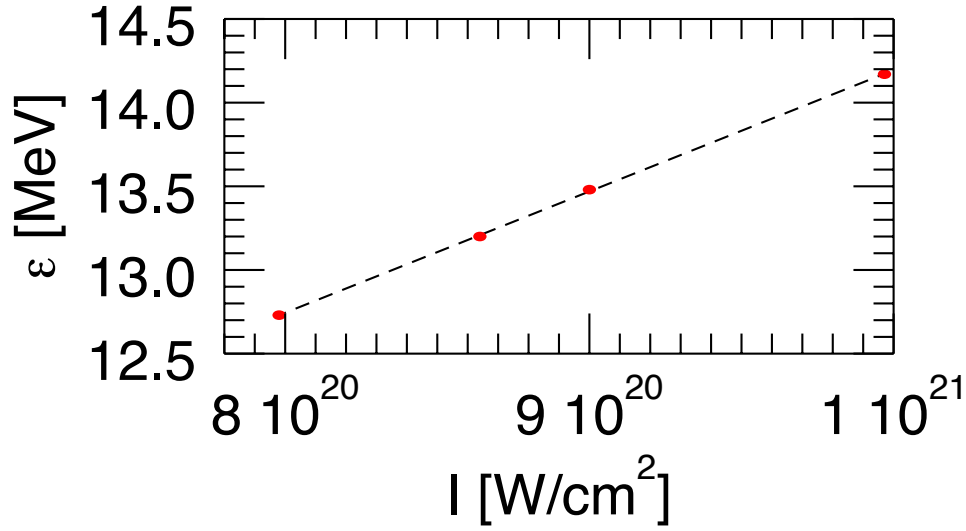
Figure 2: Proton cutoff energy at saturation vs laser intensity. These simulations consider a $6\,\mu m$ thick Al target and abrupt plasma-to-vacuum transition.

indicates that only $\sim 10^8$ protons are accelerated to energies of $15 \pm 0.5\,\mathrm{MeV}$).

The parameter scan over laser intensity was performed considering a $6\,\mu\mathrm{m}$ thick aluminium target and optimal laser contrast. These simulations suggest that, under these conditions, a more powerful laser must be considered. In particular, since the proton cutoff energy scales linearly with the laser intensity, to extend the proton spectrum beyond $20\,\mathrm{MeV}$ and accelerate sufficient protons to energies of $15 \pm 0.5\,\mathrm{MeV}$, requires laser intensities $\gg 10^{21}\,\mathrm{W/cm^2}$ (see figure 2 which shows the proton cutoff energy versus laser intensity on target).

It is essential to evaluate carefully the laser temporal profile. A sub-optimal contrast with sufficiently thick targets could pre-expand the front surface of the target leading to pre-plasma formation but leaving the rear surface of the target intact. It is well known that the presence of a pre-plasma enables more efficient electron heating mechanisms. In turn, this translates into higher proton energies. We have also considered the possibility that a pre-pulse be used to generate the pre-plasma in front of the target in a more controlled way. Preliminary simulations modelling a pre-plasma in front of the target seem to indicate that proton spectra extending beyond $20\,\mathrm{MeV}$ can be achieved with targets $> 2\,\mu\mathrm{m}$ thick and laser intensities $\lesssim 10^{21}\,\mathrm{W/cm^2}$. During the next six months, we will perform simulations to optimise the pre-plasma scale length so as to attain LhARA goals in terms of proton energy and number.

1.2.3 Update on experimental development and first beam time

Diagnostic Development:
Significant progress has been made in the development of diagnostics. Notably, we have demonstrated a version of a proton spectrometer called PROBIES (originally developed by Mariscal *et al.* [29]). The diagnostic consists of a pixelated mask of repeating filter thicknesses and a proton-sensitive scintillator layer which enables a simultaneous 2D spatially- and energy-resolved profile of the beam to be measured. The pixelated mask was 3D printed at Strathclyde and tested on both Gemini and SCAPA experiments, providing valuable insights into the behaviour of laser-driven proton beams (see figure 3). However, more work is needed to develop algorithms for the rapid de-convolution of the signal and the removal of background generated from electrons and X-rays. This work will enable operation and analysis of the proton beam profile and spectrum at the multi-Hz repetition rates
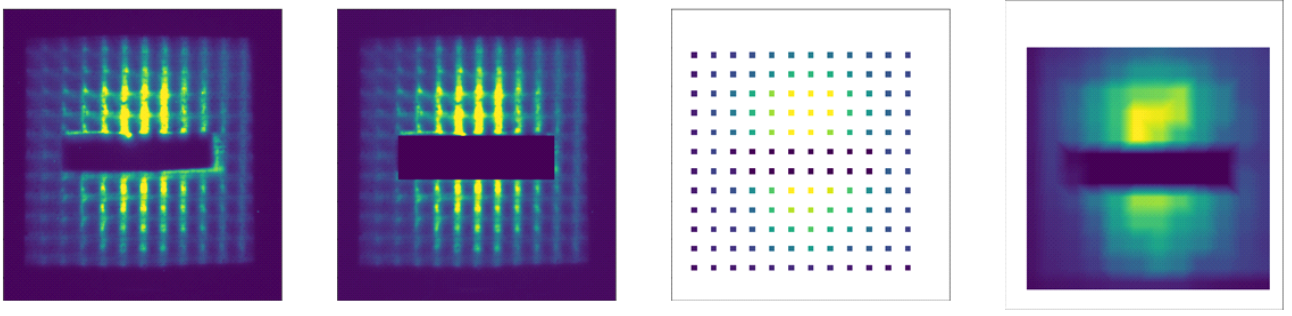
6

Figure 3: (a) Raw data recorded on the PROBIES mask (b) median filtered signal (c) individual PROBIES pixel selection (d) interpolated beam profile for 1.1 MeV pixel.

required for LhARA. Despite this, these initial experiments are highly encouraging and represent a significant step forward in our ability to measure the proton beam profile accurately at high repetition rates. In addition, we are exploring new designs that incorporate multiple scintillator layers to increase energy resolution, which could lead to a significant improvement in the energy resolution of the detector.

Targetry and Debris:

Over the reporting period, we made use of a custom tape-drive system for generating laser-driven protons and ions on SCAPA and Gemini experiments for the first time (see figure 4). With ≈1000 shots taken on each experiment, the tape drive enabled the first detailed parameter scans, providing a wealth of new data for analysis. The experiments were conducted without any serious electromagnetic pulse (EMP) issues, which were previously a concern, and the tape drive performed well on both systems. This marks a significant milestone in our efforts to reach multi-Hz repetition rates for the ion source and to gain a detailed understanding of beam properties. The data obtained from these experiments will be instrumental in advancing our research, and the successful performance of the tape drive bodes well for future experiments.

First steps have been made towards characterisation of laser debris production (see figure 5). A collaboration with the CLF has been established to make these crucial measurements during the next beam time. In addition, measurements of around 1000 laser shots were conducted on the SCAPA and Gemini laser systems, revealing the accumulation of debris on the pellicle and the PROBIES diagnostic mask. Some damage to the tape drive aperture was also observed. These findings have provided valuable indications of the nature and scale of laser-induced debris and will aid in the development of effective mitigation strategies for the ongoing progress of WP1.2. This work supports the development of both the multi-Hz operation for LhARA and the continuous operation of the source.

Data handling and control:

In the past 6 months, significant progress has been made in data handling and control for experiments on SCAPA. We developed a new version of the *DARB* software that is used on SCAPA to capture and structure experimental data. This update increases data capture rates to 1 Hz, which will enable us to collect more detailed data from laser experiments. Furthermore, changes to LPI-Py have been made to facilitate live rapid data analysis by supporting a new data analysis pipeline that stores reduced values in a live database. This will help researchers to identify trends and patterns in the data quickly during experiments. In addition, we demonstrated Bayesian optimisation of experiments using PIC simulations via the BISHOP code. The new parameters wre then used to direct the experimental shots. Development of this procedure will allow us to
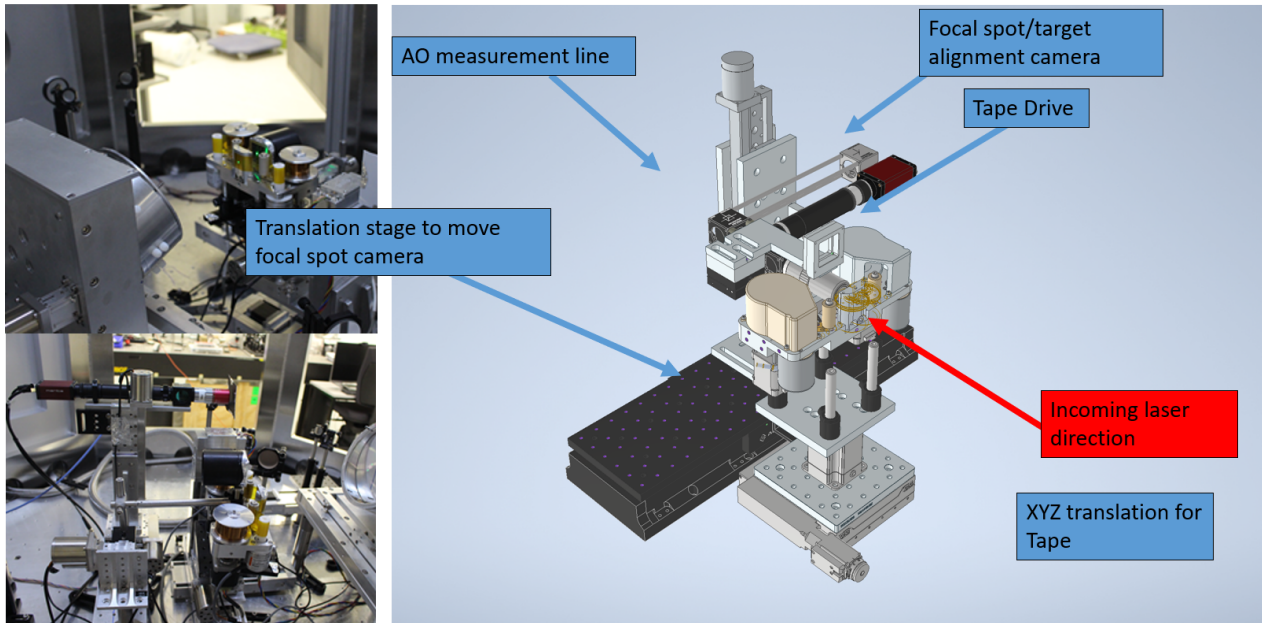
Figure 4: Images of tape drive and focal spot camera arrangement setup in SCAPA. This will support source operations at the Hz level (a) Tape drive front view (b) tape drive and focal spot camera side view (c) CAD model of tape drive and focal spot camera arrangement.
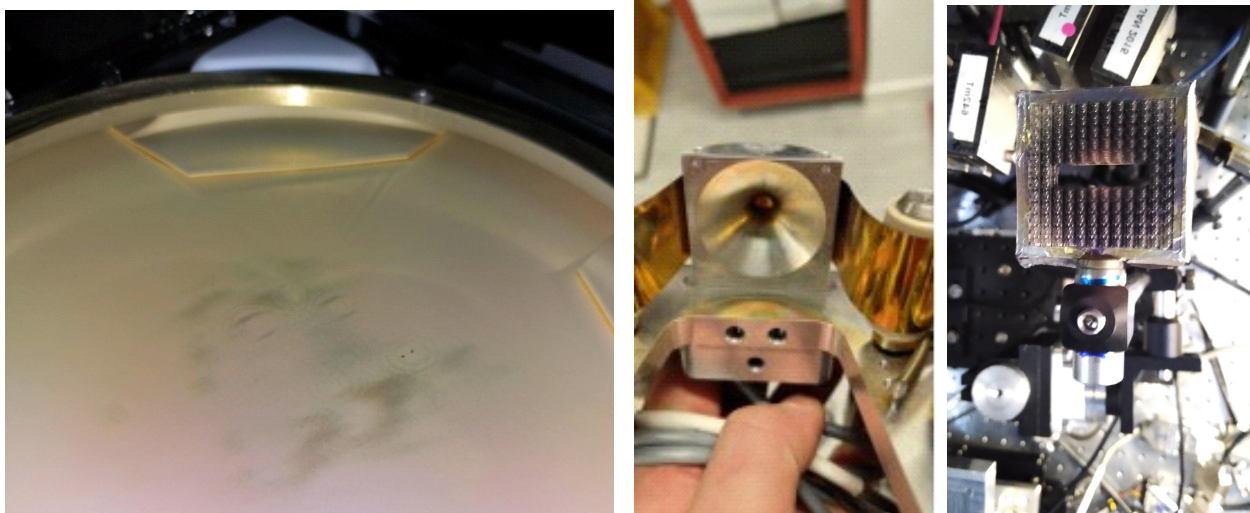

Figure 5: Images of debris build up after ≈1000 shots on Gemini and SCAPA experiments (a) Pellicle (b) face-plate for tape drive target (c) PROBIES mask.

optimise experiments more efficiently and effectively by incorporating machine learning methods to identify the most promising experimental parameters to investigate. Overall, these developments represent significant advancements in our ability to handle and analyse large volumes of data generated by laser experiments.

1.3 Work package 1.3: Proton and ion capture

Over the reporting period the key activities focused on work towards the delivery of milestone M3.1: *A report on the modification of the existing apparatus to accommodate the study of electron plasma dynamics and to validate numerical codes*, which was due at month 6. To date, our efforts have concentrated on computer simulations and the validation of different numerical codes using existing experimental results. The commercial code VSim [30] and the open-source code WarpX [31, 32] have been used following discussions with the user community. The High-Performance Computing (HPC) resources of Supercomputing Wales (SCW) have been employed to run these codes, and runtime evaluations are continuing. Progress using VSIM and WarpX is summarised in the following paragraphs.

VSim: Results and know-how developed over the past two years have been successfully transferred to the ITRF-supported team. This has allowed good progress to be made in understanding pre-supplied examples, building simulation models, and testing the performance of various models under different HPC configurations. To date, a somewhat weak (below unity) HPC scaling has been reported by SCW for several models, with clear influence by CPU number parity, nodal distribution, and wider resource use. Further evaluation is necessary.

The outputs from these tests have enabled scaling tests of collective particle motion to be performed. These outputs tentatively suggest VSim maintains strong spatial robustness when typical numerical conditions (specifically the Courant–Friedrichs–Lewy) conditions are violated, and possible Nyquist-type temporal behaviour enables a significant ($\times 50$) increase in the computational time-step to be tolerable under certain conditions. These tests are currently limited in scope as they have been performed using short-term evaluation licences.

WarpX: Due to the lack of pre-existing knowledge (both within the work package and the wider community) directly applicable to the simulations we require, progress with WarpX is less advanced. Owing to its open-source and widely-configurable nature, several WarpX work streams have been implemented to determine: the most appropriate user input configuration; the most appropriate output file format, and associated post-processing/analysis; the most efficient hardware and the best end-user implementation. The package is currently being evaluated at SCW, and validation of the code with a particle model is underway. This has so far resulted in the motion of a single particle trapped within a simple Penning-Malmberg trap to be simulated.

A generic test model is being developed with which to simulate the dynamic processes involved in loading a typical Penning-Malmberg trap with plasma via a counter-propagating 2-stream-like instability. Such a loading technique is ubiquitous within experimental apparatus and associated literature, and an efficient implementation of the technique is expected to be required for use in the final Gabor lens. Simulating this method permits a large parameter space to be investigated over extended time periods. These calculations are key to the development of confidence in the results of simulations of the long-time equilibrium of the large, high-density plasma required by the Gabor lens. The model can be configured in both the codes currently under test and will be used to determine the capabilities of the individual packages and better inform judgement of their future use.

The progress reported above has been achieved despite a $\sim 75\%$ absence of the expected workforce: specifically, the PDRA to be tasked with the execution of the numerical simulations and obtaining the corresponding physical data from existing apparatus. Suitable candidates have recently been identified following an interview

9

process, although they are not currently expected to begin activities before Summer 2023. Milestone LhARA M3.1 is now scheduled to be completed by the end of December 2023.

1.4   Work package 1.4: Real-time dose-deposition profiling

LhARA work package 1.4 (WP1.4) has two objectives for the current Preliminary Activity:
- O4.1 the development of the Geant4 [33] Monte Carlo simulation component of the forward model; and
- O4.2 the development of the k-wave [34] simulation component of the same forward model.

These activities together enable the principal task for the Preliminary Activity phase, which is the detailed design, including identification of potential suppliers of components, of an experiment to prove the principle of ion-acoustic dose-profile measurement. No researchers were resourced for WP4 in the current grant, the work instead being carried out by research students leveraged from outside the Preliminary Activity funding. With reference to the tasks defined in the Gantt chart of Table 8 of CCAP-TN-10 Annex "Scope of work to be carried out under the ITRF Preliminary Activity" [4], progress during the current 6-month reporting period is summarised in the paragraphs that follow.

1.4.1   Review

The initial review of the literature on the applicaiton of ionacoustic dose-profile measurment is complete, and may be found in masters theses and reports from Josie McGarrigle, Anthea MacIntosh-LaRocque and Maria Maxouti [35, 36]. Papers published since these reports were completed have been discussed at biweekly meetings of the group [37]. Overall, encouraging results have been presented by other groups indicating ionacoustic signal detectability in a water bath and *in vivo*. A superior signal-to-noise ratio is expected from LhARA. Our workplan, including signal bandwidth studies and reconstruction algorithm development, remains novel and promising.

1.4.2   Monte Carlo part of the forward model

Simulation of current beamline and smart phantom:
A collaboration was established with the groups led by Professors Katia Parodi and Jörg Schrieber at Ludwig-Maximillian University (LMU), Munich, with a view to exposing the SmartPhantom to the proton beam delivered by the laser driven "LION" beamline on CALA at LMU. BDSIM was used to simulate the LION beamline using a parameterisation of the spatial and energy spectra produced by the source. A pair of orthogonal quadrupole magnets is used for focusing. The source has a broad proton energy distribution falling exponentially to a maximum around 25 MeV. Protons of 20 MeV are focused into the SmartPhantom and create a Bragg peak at a depth ~ 4 mm. Geant4 has been used to simulate the SmartPhantom, which is modelled as an aluminium box with a Kapton entrance window at the end of a cylindrical air-filled port into the phantom, producing a 3D deposited-energy distribution for use as the input to the k-Wave part of the forward model (see below).

Four planes of scintillating fibres, an essential part of the design of the planned validation experiment, have been incorporated in the Geant4 simulation. Each plane consists of 33 polystyrene fibres each of length 10 mm, 250 μm diameter, with a pitch of 300 μm, forming a sensitive area of 10×10 mm^2. The simulated energy deposition in the fibre array suggests that up to 5 fibres will be illuminated by the beam. With fibre planes positioned at about 0, 1, 2 and 3 mm from the detector centre, the Bortfeld equation [38] provides a good fit to the scintillation signal, representing an excellent pulse-specific reference against which to compare the

deposited-dose axial profile reconstructed from the ionacoustic signal. Prototype scintillating-fibre planes have also been successfully constructed to this design, with fibres wound on plastic and aluminium frames. Future work includes finishing this construction, testing the fibre planes with a proton beam, and finally using them in an experiment to validate the simulations with data.

Work has been initiated to explore the possibility of using liquid scintillators in the SmartPhantom, and reconstruction of the dose distribution from multi-view optical cameras, to overcome the likely acoustic-wave disruption that would be caused by the fibre planes, given that a pulse-by-pulse validation is likely to be desirable.

An MRes Cancer Technology project has been set up between the Institute of Cancer Research (ICR) and Imperial College London to explore an additional simulation validation experiment. The intention is that this will employ the output of the Geant4 simulation to 3D print a thresholded version of the deposited-dose distribution as a plastic mould. The mould will be used to create pigmented gel phantoms in the shapes of outlines of the dose distribution at various threshold values. Each of these will then be imaged using a photoacoustic imaging system at the ICR. Study of the signals and reconstructed images, in comparison with k-Wave equivalents, for various threshold values will allow validation of the forward model allowing further understanding of the overall acoustic signal's time-frequency composition to be gained for sensor elements placed in various locations and for various proton beam energies.

Updated simulation of LhARA and smart phantom:
Due to start in Q4 of 2023.

1.4.3   k-Wave part of the forward model

Simulation of ionacoustic source, propagation and sensing, and design of array configuration for validation experiments:
For a preliminary demonstration of the full simulation pipeline, the above 3D deposited-energy distribution was assumed to exist for 40 ns with instantaneous rise and fall. When converted to an acoustic source pressure distribution using a Grüneisen parameter for water, this rate of change of deposited energy was used as the source in a k-Wave simulation. Convergence tests demonstrated that a k-wave finite element mesh of 0.1 mm voxels is sufficient for accurate simulation of the acoustic source and the propagating acoustic wave at this proton energy. Movies of the wave travelling away from the deposited-energy distribution showed wave directions and rates of decay in a lossless medium (water) qualitatively consistent with a cylindrically diverging wave along the radial direction upstream of the Bragg peak, and pseudo-spherical divergence from around the Bragg peak, due to the proton beam flaring due to energy straggliong and small angle scattering. Inward propagating waves were also seen from the boundaries of the deposited-energy distribution, as expected. These phenomena will influence the bandwidth of the acoustic waves and hence of the acoustic sensor array design, and their further study is an important next step. Temporarily, to complete the preliminary test of the full simulation pipeline, an array consisting of 300 acoustic sensor elements, each a 2 mm diameter disc, were placed on a hemispherical surface of 7 mm diameter positioned with its centre about 2 mm upstream of the Bragg peak. This simulation allowed several potential dose-map reconstruction algorithms to be tested under noiseless conditions (see 4.4 below).

Updated simulation of ionacoustic source and development of sensor array specification, as LhARA specifications are developed in other work packages:
Due to start Q4 of 2023.

1.4.4 Implementation, simulation evaluation and development of inverse dose-map reconstruction software

Direct ionacoustic reconstruction with handling of sensor array configurations:
Due to start Q2 of 2023. Nevertheless, progress has been made with the aim of demonstrating the functionality of the full simulation pipeline. Using the sensors arranged in a hemispherical array (section 4.3.1 above), three image reconstruction methods were evaluated: iterative time reversal, model-based minimisation, and direct back-projection. Iterative time reversal appeared to provide a 3D dose-map reconstruction whose shape most closely approximated that of the original deposited-dose distribution, with a shape around the Bragg peak that converged on correct shape after four iterations, underestimating the Bragg peak when fewer iterations were used. Model-based minimisation required more iterations (>5) and never fully converged in the study so far. Back-projection is a rapid non-iterative method and directly provided a result similar to the first iteration of time reversal and arguably superior to the first iteration of the model-based minimisation method. All methods failed to produce an adequate representation of the deposited-dose distribution at beam depths considerably upstream of the hemispherical centre, although this was expected as this region is out of the field of view of the hemispherical detector array, and could be corrected by mechanical motion of the array in any final device, or by compromising on resolution for extended field of view using other shapes of array and/or other sizes and number of elements.

Iterative reconstruction methods with model-based priors:
Due to start Q2 of 2024.

Iterative reconstruction methods with angular dependence of frequency content:
Due to start Q4 of 2024.

Implementation of various dose-map reconstruction programs on Verasonics system:
Due to start Q2 of 2024.

1.5 Work package 1.5: Novel, automated end-station development

Over this reporting period we have made progress on all milestones and deliverables defined in [5]. Dr. Narender Kumar has been appointed by the University of Liverpool and a new PDRA appointment will be made shortly to complement this effort. A PhD studentship has been secured via EuPRAXIA-DN [39] to work on the diagnostic challenges directly related to LhARA. Dr Kumar is currently performing an extensive literature review of beam diagnostic techniques for ultra-high-dose-rate beams in order to identify any potential technologies or R&D areas in preparation for the milestone report due for month 12. Work has also begun on adapting the gas profiler, identified as a potential diagnostic tool, which is minimally disruptive to the beam and allows monitoring of the beam intensity, profile, and energy. A successful application to the University of Liverpool Faculty Impact Scheme for £15k will allow gas-profiler measurements of protons and carbon ions during the summer of 2023 at the Dalton Cumbria Facility in Whitehaven.

The first peer-group consultation meeting was organised and took place in December 2022. Due to national train strikes, the meeting was conducted fully online, advertised at a national and international level; it attracted more than 50 registrants. The first consultation meeting primarily focused on the low-energy *in-vitro* beamline for LhARA, with discussions also on the high-energy *in-vitro* and *in-vivo* end stations. Key talks were presented by collaborators from within the LhARA/ITRF community and by experts external to the collaborations [40]. The talks informed the community of the vision of the LhARA/ITRF programme. Interactive sessions were

held in the afternoon to gauge interest, listen to views, identify requirements, and to discuss key beam and experimental parameters. The general consensus from the meeting was that the LhARA facility would offer benefits over existing facilities and that going forward more focus should be placed on:

1. The radiobiological opportunities arising from the unique time structure that LhARA offers;

2. The experimental complications arising from using a low-energy proton beam; and

3. The workflow and required cell-culturing facilities required to support a multi-user, quasi-continuous irradiation facility.

These points will form the basis of future discussions as they will have impact on both the high- and low-energy operations, the end-station apertures, building designs, automation, and beam diagnostics.

A key design decision—made based on the input from the first consultation meeting—is that the LhARA baseline should not be revised; i.e., that the *in-vitro* beamlines should remain vertical whilst the *in-vivo* beamline should remain horizontal. The design of the facility is required to accommodate this and requires the specification and design of each end-station. The community of potential users prefers to be able to keep cell dishes horizontal to avoid the need to seal the dishes and reduce the potential mixing of drugs, inhibitors, markers, or other biologically relevant substances in the dishes which may impact on the biological results. This choice has an impact on the orientation of all systems within the end station and will be factored into design work. The 35 mm diameter beam offered in the low-energy *in-vitro* LhARA end station will be sufficient to irradiate samples but there is interest in smaller beams for spatially-fractionated studies. An upper limit on the accuracy of the dosimetry was agreed to be 5%, such that radiobiological factors will contribute the dominant uncertainty in the measurements. In keeping with this, dose repeatability at the level of 5% across multiple cell dishes was preferred. However, provided dosimetry is available for each dish, this repeatability criterion can be relaxed and the measured dose factored into subsequent analysis. This requirement highlights the need for the end stations to be compatible with appropriate dosimetry techniques such as that being developed in LhARA Work Package 1.4 and those identified during the course of this project.

A report on the first consultation meeting is in preparation. In preparation for the second meeting, a questionnaire will be sent to all attendees of the first consultation meeting to ensure that all of their requirements have been collected and recorded. The next consultation meeting will focus on the low-energy *in-vitro* end-station; the other end stations will be discussed in future meetings. Therefore, the initial report for LhARA M5.1 will only include information on the low-energy *in-vitro* end station. Planning for the full sequence of consultation meetings to be carried out during the Preliminary Activity is underway. The outcomes from these meetings will be reflected in the report that will be prepared to meet milestone LhARA M5.3.

Work has begun on the University of Birmingham MC40 cyclotron high intensity facility. An experiment has been conducted using a 28 MeV proton beam incident upon the NPL Secondary Standard Calorimeter which demonstrated that dose rates in excess of 2.5 kGy/s are possible. Geant4 simulations have been conducted to study the impact of beamline components, including vacuum windows and current monitors, on the profiles and energy of a 15 MeV proton beam. Studies are underway to optimise the MC40 procedures to measure the proton energy and to allow a large uniform beam, with minimal losses at the facility in order to maximise the potential dose rate over a larger area for cell irradiations.

1.6 Work package 1.6: Facility design and integration

1.6.1 Review of current baseline

It is proposed that the LhARA facility, shown schematically in figure 6, will be implemented in two stages: Stage 1 will serve the low-energy *in-vitro* end station with proton beams with energies up to 15 MeV; and
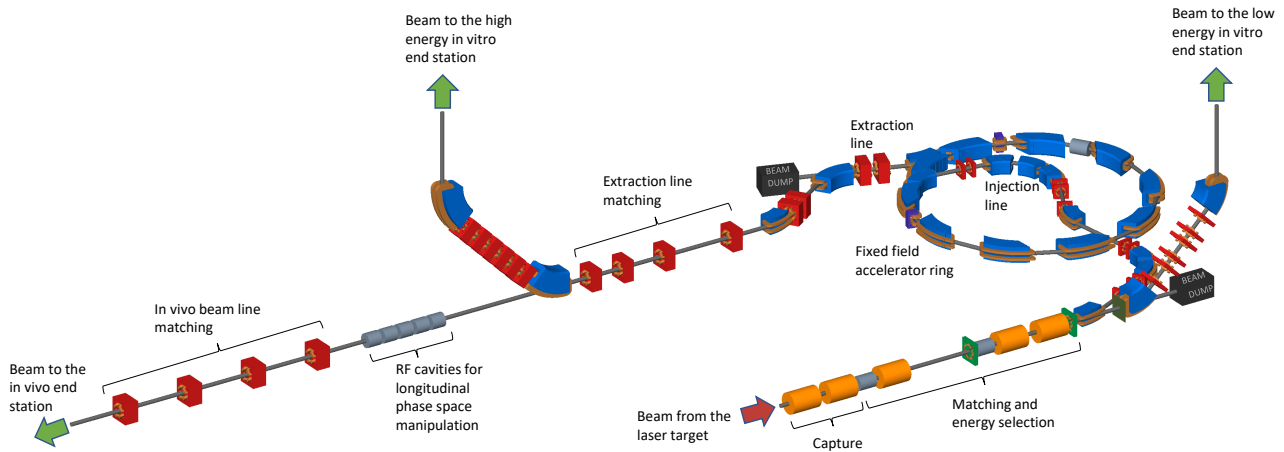
Figure 6: Schematic diagram of the LhARA beam lines. The particle flux from the laser-driven source is shown by the red arrow. The 'Capture' section is followed by the 'Matching and energy selection' section. The beam is then directed either into the $90°$ bend that takes it to the low-energy *in-vitro* end station, towards the fixed-field accelerator injection line, or to the low-energy beam dump. Post acceleration is performed using the FFA on extraction from which the beam is directed either to the high-energy *in-vitro* end station, the *in-vivo* end station, or the high-energy beam dump.

Stage 2 will serve the high-energy *in-vitro* end station and the *in-vivo* end station with proton beams with energies of up to $127\,\text{MeV}$ and ion beams, including C^{6+}, with energies of up to $33\,\text{MeV/u}$. A detailed description of the current baseline is maintained in [41].

At Stage 1, the transport line downstream of the laser source consists of five Gabor lenses and a vertical $90°$ arc that delivers beam to the low energy *in-vitro* end station. The first two Gabor lenses capture the highly divergent flux generated by the laser source, performing a point-to-parallel transformation. Following the capture section, a shielding wall will separate the target/capture room from the downstream accelerator sections. Following the shielding wall, a drift section will host diagnostics and an RF cavity for phase rotation. A third Gabor lens then focuses the beam into the first collimator at which the desired beam-energy bite is selected. The collimator is followed by a second RF cavity which is used to control the bunch length. Diagnostic devices, correctors and an octupole magnet used to control the spatial uniformity of the beam, are to be placed in the drift between the third and the fourth Gabor lenses. The fourth and the fifth Gabor lenses form a matching section to prepare the beam for the vertical arc or for transmission to the fixed-field accelerator. The drift that follows the fifth Gabor lens contains an octupole, a second collimator, and a switching dipole which, if energised, will send the beam into the injection line for Stage 2. When the switching dipole is not energised the beam will be transferred to the vertical arc which consists of two $45°$ bends and six quadrupoles. The arc includes a second collimator to select momentum. This collimator exploits the dispersion created by the first dipole. The arc is designed to be a first-order achromat matching dispersion to zero and with a phase advance of $n\pi$, where n is an integer in both transport planes. Beam transport through the arc may therefore be described by an identity transformation. When the first $45°$ dipole is not energised the beam will be sent to the low-energy dump. The beam line for Stage 1 is shown in figure 7.

The Stage 2 accelerator system consists of the injection line feeding the fixed-field accelerator (FFA), the high-energy beam transport line, the high-energy beam dump, a second $90°$ arc to deliver the beam to the high-energy *in-vitro* end station, the beam transport line, and the beam matching section serving the *in-vivo* end station.
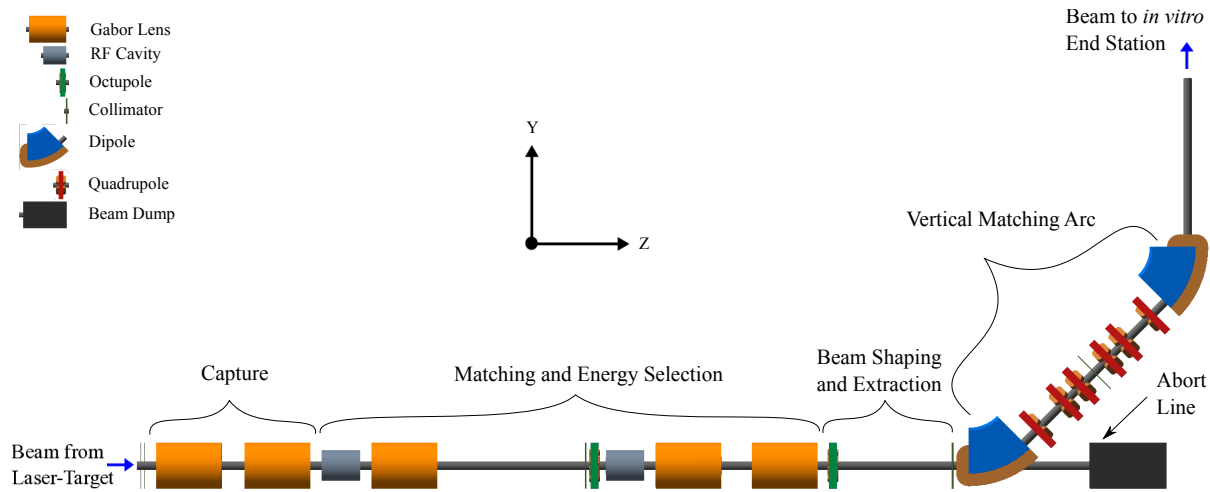
Figure 7: Schematic diagram of the baseline design of LhARA Stage 1 beam line.

1.6.2 Infrastructure

The building and technical infrastructure will require careful planning, design and implementation to ensure the facility delivers on its challenging scientific objectives and provides accommodation that inspires scientific research. The overall success of the facility requires an integrated approach for the high-power laser, target, capture, matching and energy selection of ions, accelerator, end stations, control rooms, building, services, as well as staff and user needs such as preparation laboratories, offices, meeting rooms and amenities. The needs of all stakeholders must be solicited and taken into account from an early stage of the project to ensure that the facility design and implementation plan meets the requirements. This section describes the progress made over the first 6 months of the ITRF project in the development of the conceptual design of the building and its contents. The conceptual design will be further developed to deliver the full conceptual design by September 2024. The need for equipment stability will be crucial and will require stringent control of vibration, floor stability and environment control in key areas. The vision is to construct a new, purpose-built, energy-efficient facility in terms of its construction, operation and decommissioning. The facility conceptual design floor plan, that has been developed to meet the science requirements, is shown in figure 8. The facility begins with proton and ion beams which are generated when a high-power titanium-sapphire (Ti:S) laser impacts upon a target.

There are three experimental end stations, each with a local control room. Two end stations will be used for *in-vitro* experiments, indicated in red text on figures 8 and 9. These end stations are located on the first floor above the accelerator complex at the end of vertical beam lines (see figure 10). Post acceleration is provided by the FFA in Area 4. The *in-vivo* end station is located on the ground floor in Area 6.

The site plan has been laid out on an area estimated at $72 \times 32\,\mathrm{m}^2$, of which $57 \times 32\,\mathrm{m}^2$ is the footprint of the main building, next to which a $15 \times 32\,\mathrm{m}^2$ exterior fenced pen houses the water cooling chillers, water storage tank, water pumps and transformers, see figure 11. The exact capacity of these systems will be estimated when more precise details of the facility equipment are defined. The water-cooling equipment location has been chosen to be close to the heat exchangers and equipment with a high cooling load. Similarly, the transformer(s) and main electrical switchboard are located close to each other to reduce the length and cost of interconnecting cables. A 2.5 m wide access margin around the circumference of the accelerator is proposed to provide fork-lift access to equipment.

A cross section through the building is shown in figure 12. The overall height is estimated to be 14 m to
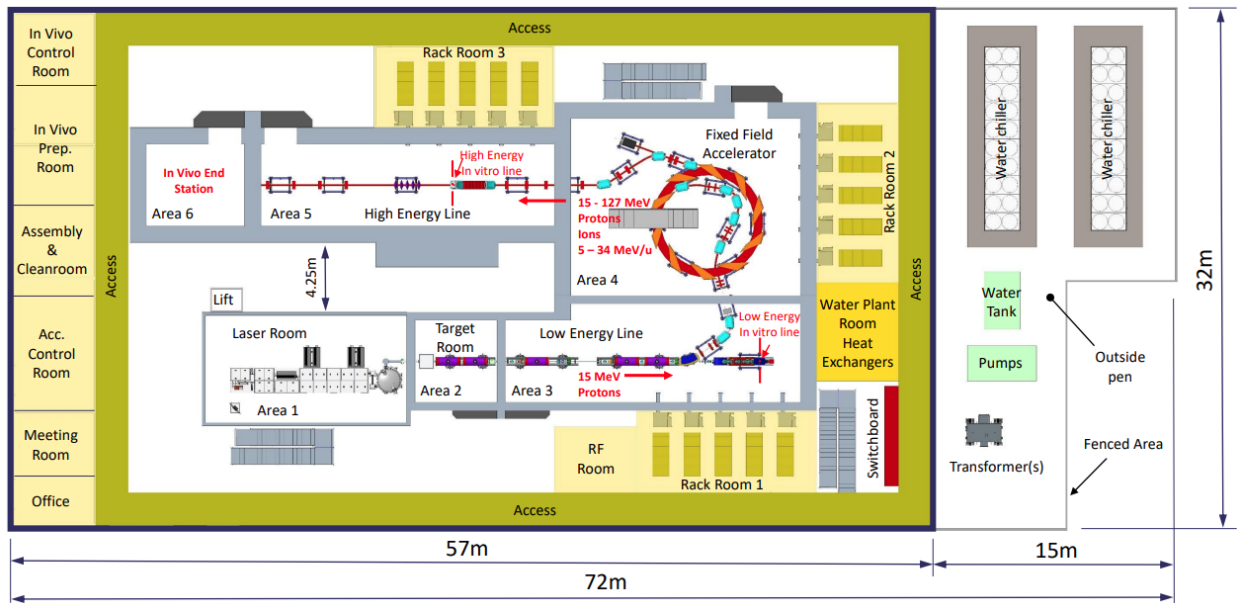
15
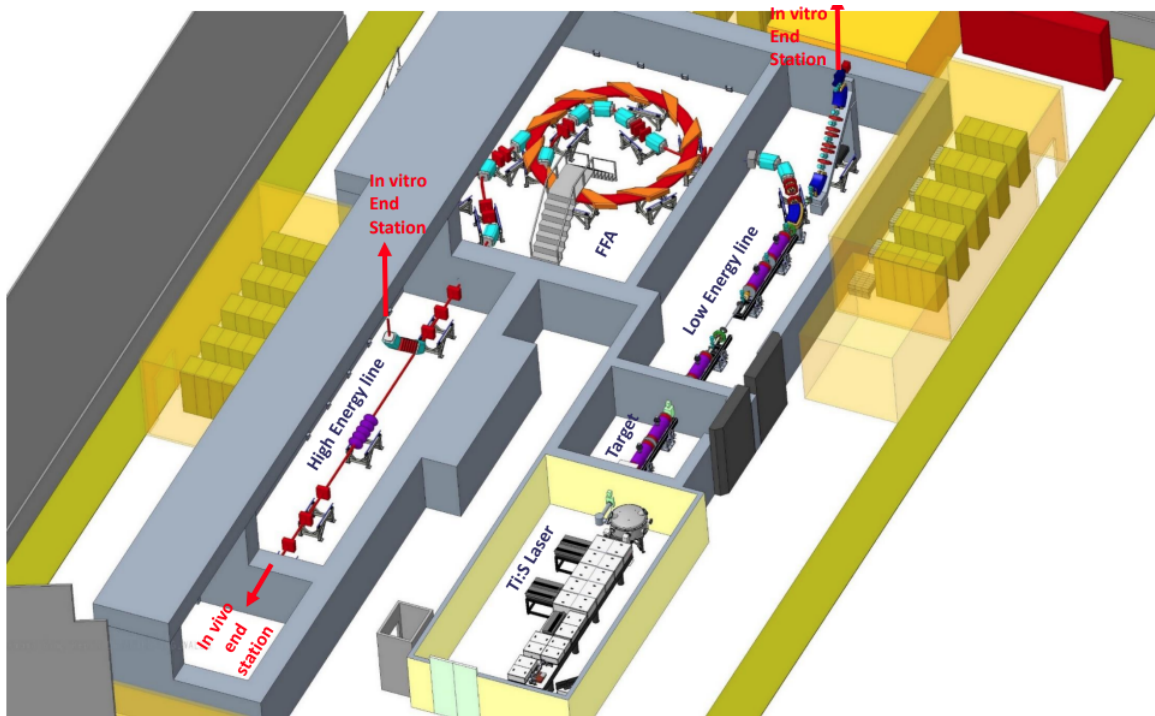
Figure 8: Facility ground floor plan.

Figure 9: Accelerator complex with shielding cut away to see equipment. Three end stations are shown, indicated with red text.
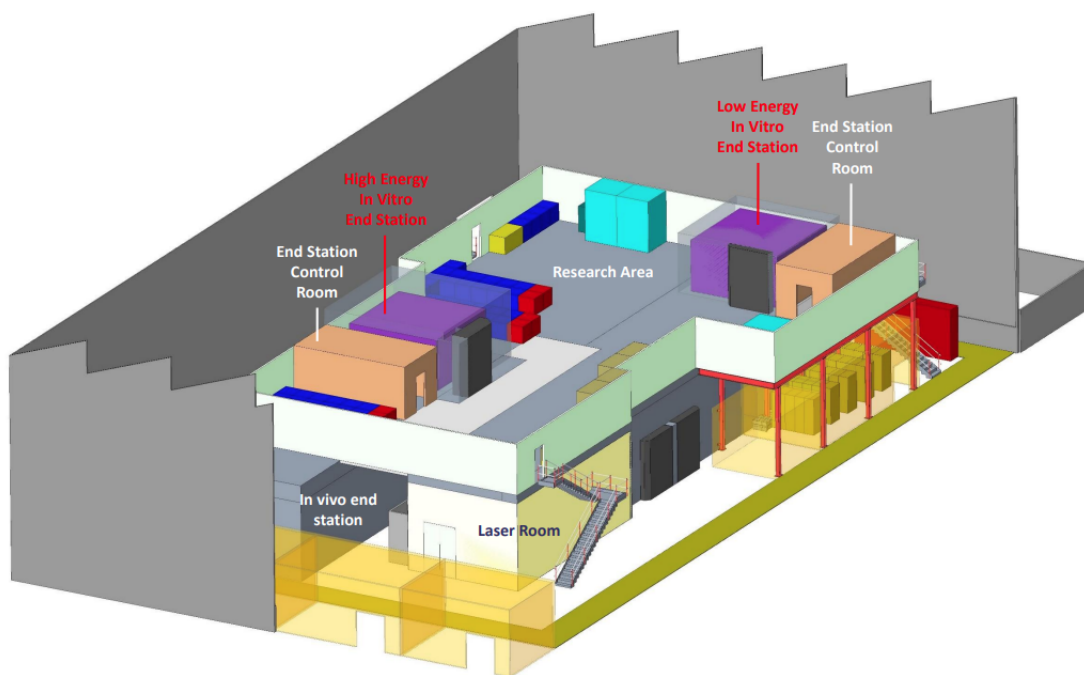
Figure 10: End stations and research area above the accelerator complex on the 1st floor.
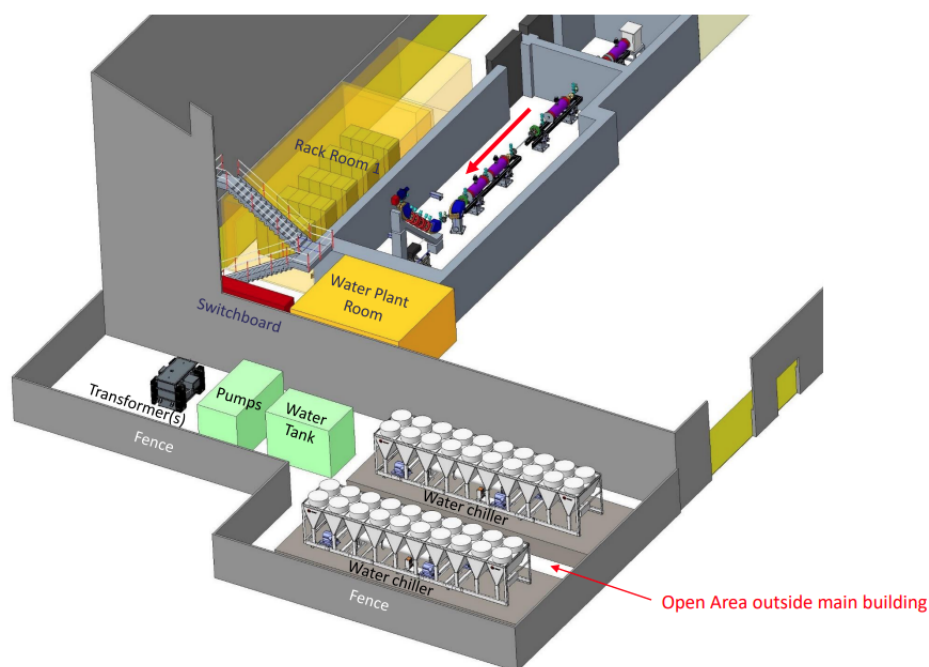

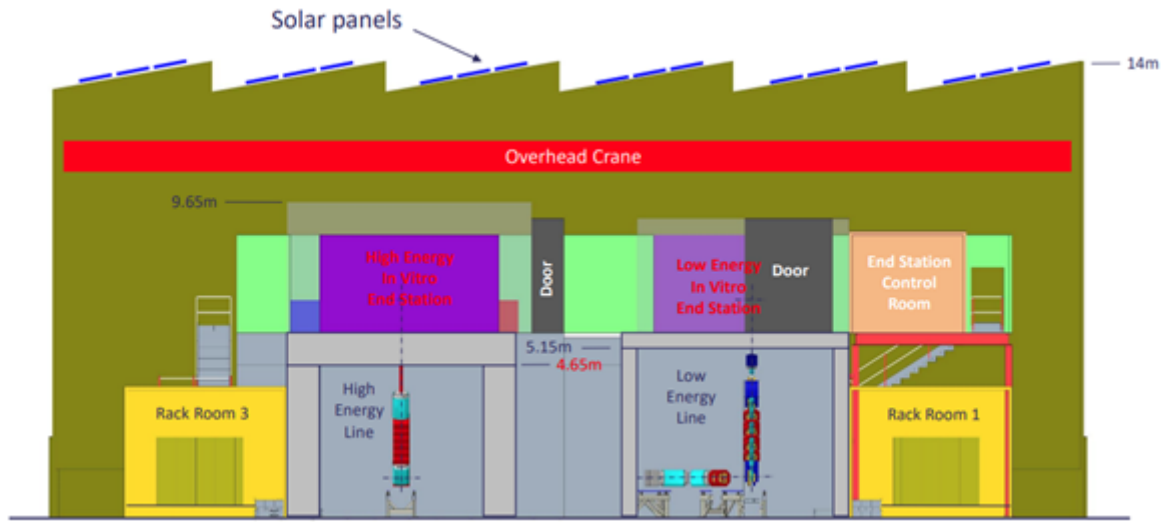Figure 11: Water cooling plant and transformer(s) outside pen.

Figure 12: Cross section through the facility.

allow the implementation of an overhead crane both to install and decommission the facility. Lifting solutions will also be required inside the radiation enclosures for installation, maintenance and decommissioning. For installation, maintenance and decommissioning of the vertical beam lines, permanently-installed platforms next to the accelerator components are envisaged to provide a safe and efficient working environment. Sliding shield doors are shown in the figures but labyrinth access will also be considered during the technical design stage. A saw-tooth roof construction is proposed comprising of a series of ridges with dual pitches. The steeper surfaces at $\sim 70°$ are proposed to have double-glazed windows to admit natural light. The shallower surfaces at $\sim 35°$ are proposed for the installation of solar panels facing south to receive the most direct sunlight. Two sets of stairs and a lift are proposed for personnel and the transport of light equipment. Heavy items could be lifted to the accelerator complex roof with the overhead crane.

For the accelerator systems shown on the ground floor, 60 power supply, control, and instrumentation racks are currently estimated to be required (see table 2). Their locations are shown on the ground floor of the facility in figure 8. This estimate will be updated as more detailed technical specifications are generated. The racks will be located in three insulated air-conditioned rooms to minimise dust and to provide temperature control for the stability of the power supplies.

Table 2: Ground floor power supply, control & instrumentation rack rooms.

Rack Room	Equipment	No of racks
1	Low Energy Line	20
2	Fixed Field Accelerator	20
3	High Energy Line & *in-vivo* End station	20

It is proposed that the laser room will contain an internal technical corridor to house power supplies; this thereby reduces heat dissipation in the vicinity of the laser, which has a stringent temperature stability requirement of $20 - 22°C$ to better than $\pm 1°C$ monitored at less than $2\,m$ from the optical tables. The laser room also requires humidity of $40 - 50\%$, to be monitored less than $2\,m$ from the optical tables, and cleanliness to ISO class 7 [42].

Area	Description	Size (m×m)
1	100 TW laser room	12.3×6.5

Table 3: Laser room size.

1.6.2.1 Radiation Safety

The accelerator complex on the ground floor is proposed to be divided into six areas to provide flexibility for the construction, maintenance and operation of the facility. By segregating the controlled areas shown in figure 8 and Figure 10, access to downstream rooms will be possible when ion beams are operating in the upstream controlled areas. This flexibility will allow the project construction duration to be reduced significantly by allowing systems commissioning with beam in parallel with installation of downstream areas, for example operating the Stage 1 low-energy line while installing the Stage 2 FFA. Faster maintenance and checks are also possible with the facility separated into functional areas because the full accelerator complex will not have to be searched, as would be the case were all accelerator equipment to be installed in one large area. To achieve this flexibility, radiation shutters will be required to cover each beam aperture in the shielding walls. The shutters will be interlocked to the access doors and both the doors and shutters will be controlled within the personnel safety system.

The thickness of the bulk shielding shown in figure 8 and figure 10 has not been determined. A specialist company will perform a radiation study during Q1 and Q2 of 2024. The radiation study will include the following activities:

- A high-level shielding design report that creates a point of reference for all the shielding protection calculations;
- Radiological classification of areas;
- Preliminary bulk shielding requirements; and
- Concrete sustainability appraisal.

Table 2 lists the rooms that make up the ground floor accelerator complex. The 100 TW laser room is specified to be constructed with thermally insulated panels, the dimensions of which are given in table 3. Areas 2–8 form the radiation shielded enclosures. To reduce the volume of concrete required, the implementation of composite shielding, consisting of a concrete skin filled with magnetite aggregate, is being considered. Such a solution has been used in the CALA facility [43] based on previous constructions by Forster [44]. The construction technique is significantly more sustainable than a conventional cast-concrete solution due to the substantial reduction in the volume of concrete required. A further development of this technique, in which shielding blocks are constructed using the composite technique, is being considered. Shielding blocks provide flexibility and allow cost-effective upgrades and simplification of staged installation and decommissioning. The ability to re-use shielding blocks many times on future facilities further improves sustainability and value for money after the lifetime of the proposed facility.

1.6.2.2 Designation of Areas

IRR17 [45] requires an area to be designated as a "controlled radiation area" if a person entering that area is likely to receive an annual dose in excess of 6 mSv, or if they are required to follow special procedures intended to restrict their radiation dose or the effects of an accident. The radiation hazard inside the shielded enclosures will generally be negligible when they are not interlocked by the Personnel Safety System (although consideration must be given to components such as collimators and beam dumps which have the potential for

Table 4: Facility room sizes. Areas 2–8 require radiation shielding and are identified as controlled areas.

Area	Description	Internal room size (m×m)
2	Target room	5×5
3	Low energy line room	18×6
4	Fixed field accelerator room	14×10.8
5	High energy line room	18×5
6	*in-vivo* end station	6×5
7	Low energy *in-vitro* end station	5.5×5.5
8	High energy *in-vitro* end station	5.5×5.5
9	Low energy *in-vitro* end station control station	6.8×3.4
10	High energy *in-vitro* end station control station	6.8×3.4

high levels of induced activity after the ion beam has been switched off). Adopting the model used at similar facilities, areas 2–8 in table 4 will be designated as controlled radiation areas on a permanent basis. IRR17 defines a "supervised radiation area" as one where it is necessary to keep the conditions of the area under review to determine whether it should be designated as "controlled" or where a person is likely to receive an annual dose in excess of 1 mSv. It is therefore proposed that the surroundings of the accelerator complex are designated as supervised radiation areas, at least for an initial period whilst environmental dose measurements are taken in the surrounding areas within the facility building.

1.6.2.3 Personnel Safety System

The Personnel Safety System will be similar to that in use on the existing UKRI-STFC facilities in that it will be compliant with IRR17 and the Accelerator Code of Practice in accordance with IEC61508 [46]. The architecture of the system will be subject to the analysis of the hazards and probabilistic modelling of safety issues to achieve the target safety levels for the facility. The design of the system will be advised by current "best practice" for accelerator access-control and key-exchange systems, and will include the requirement for shielded areas to be searched prior to operation of the facility. The processes necessary to comply with IEC61508 includes the following requirements:

- Identify the acceptable safety levels required for the facility;
- Identify the hazards using a technique such as HAZID including severity, initiating event, frequency of occurrence, non-EEPE control measures and EEPE control measures. (HAZID: HAZard IDentification study; EEPE: Electrical, Electronic and Programmable Electronic safety system);
- Identify (from the HAZID) the functional requirements for EEPE;
- Model the safety requirements to generate probabilistic requirements for the safety functions, leading to SIL rating. (SIL: Safety Integrity Level);
- Undertake detailed design work;
- Review the design work with respect to functions;
- Build the Safety System;
- Test functional performance with respect to functional specification;
- Undertake proof tests to ensure continued correct operation; and
- Collect data and review performance against the assumptions in the safety model and HAZID.

A safety system that is compatible with IRR99 [47] and the "generic prior authorisation" will include:

- Hierarchy of control measures;
- "Emergency Off" buttons ;
- Search systems;
- Key transfer system, with the ability to leave the system disabled;
- "Fail safe" annunciators (signs);
- Tests at suitable intervals; and
- Maintenance.

The system is also likely to include:

- PA announcements;
- Blue lights;
- Other warning signs;
- Redundancy and diversity of safety control measures; and
- Redundancy and diversity of safety systems.

1.6.2.4 Staged Construction

The site at which the proposed facility will be constructed has not been chosen, but it has been discussed that the facility may benefit from being built at a UKRI–STFC National Laboratory site to take advantage of existing infrastructure and facilities, the availability of multidisciplinary technical staff, approved radiation site authorisation, and large electrical-power capacity.

It is proposed that the construction of the facility will be in two stages:

- Stage 1 providing beam to the low energy *in-vivo* end station shown in figure 13 and figure 14. Stage 1 will require the implementation of the:
  - Full building;
  - Full fenced outer pen to house the water cooling systems and transformer(s);
  - Laser room
  - Radiation shielding for areas 1 – 3 and low energy end station;
  - Laser, accelerator and end station technical systems for the:
    * Laser-driven proton and ion source;
    * Proton and ion capture section;
    * Matching and energy selection section;
    * Low energy abort line; and the
    * Beam delivery to low-energy *in-vitro* end station;
  - First-floor research area for Stage 1;
  - Low energy *in-vitro* end station systems;
  - Low energy *in-vitro* end station control room;
  - Rack room 1;
  - RF room;
  - Main switchboard;
  - Internal water plant room containing heat exchangers and pumping;
  - General technical services for the above described systems including electrical distribution, water cooling distribution, HVAC, compressed air and gases;
  - Accelerator control room, meeting room, cleanroom and general office;
  - EPICS control system for above systems;
  - Personnel safety system; and the
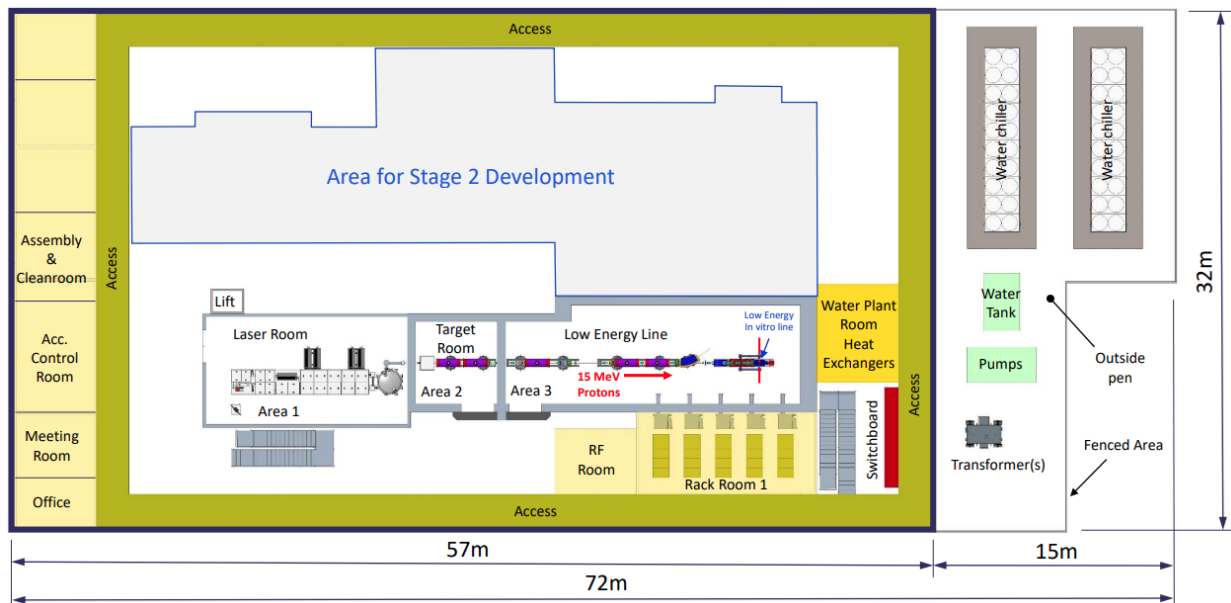 - Two sets of stairs and light duty equipment lift to level 1.

Figure 13: Stage 1 floor plan.

- Stage 2 delivering the full functionality of the facility shown in figures 8–9 requires the further implementation of the:
  - Accelerator and end station technical systems for:
    * Fixed field accelerator;
    * High energy extract line;
    * High energy abort line;
    * Beam delivery to high energy *in-vitro* end station; and
    * Transfer line to the *in-vivo* end station;
  - Radiation shielding for; areas 4 – 6, high energy *in-vivo* end station and *in-vivo* end station;
  - High energy *in-vitro* end station systems;
  - High energy *in-vitro* end station control room;
  - *In-vivo* end station;
  - *In-vivo* control room;
  - *In-vivo* experiments preparation room;
  - 1st floor research area rearrangement for Stage 2;
  - Rack room 2 and 3;
  - General technical services for the above described systems including electrical distribution, water cooling distribution, HVAC, compressed air and gases;
  - EPICS control system for above systems;
  - Upgrade to personnel safety system;
  - Upgrade to accelerator control room; and
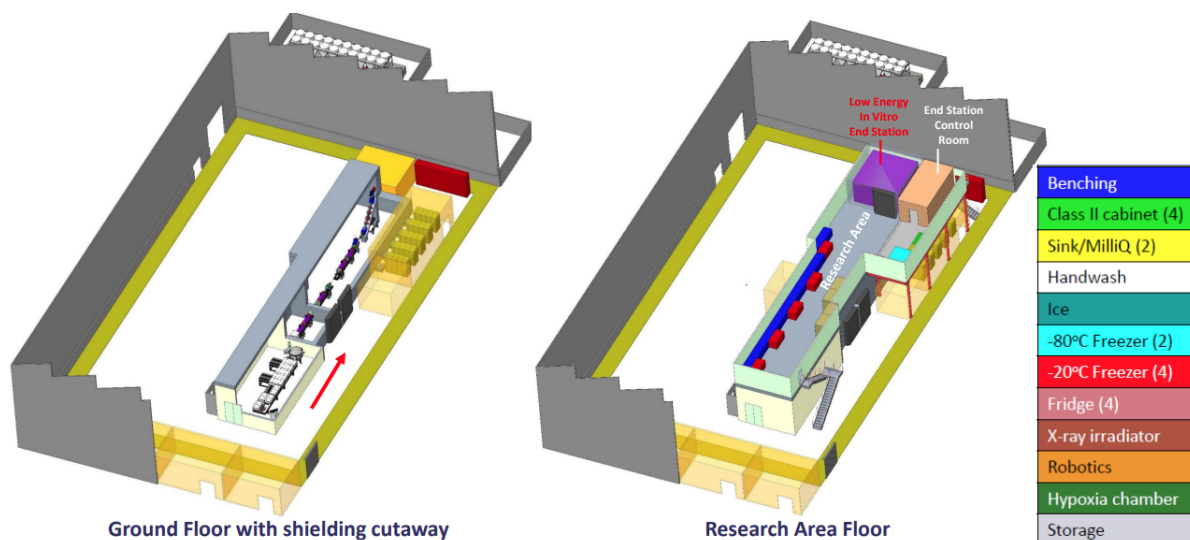 - Third set of stairs to level 1.

22

Figure 14: Stage 1 construction.

1.6.2.5 Key Installation Milestones

The installation and commissioning of the LhARA systems will be coordinated so as to maximise the scientific output of LhARA. Thus, prior to the completion of construction, the goal will be to achieve the following scientific milestones:

- Stage 1
    - First demonstration of the capture of a laser-driven ion beam using a Gabor lens system;
    - Demonstration of the energy selection capabilities of a Gabor lens system; and
    - Irradiation of cells with a laser-driven ion beam.
- Stage 2
    - Injection line to the FFA;
    - Fixed Field Accelerator;
    - Extraction line from the FFA and the transfer line to the *in-vivo* end station;
    - High energy *in-vitro* arc;
    - High energy *in-vitro* end station; and
    - *In-vivo* end station.

1.6.2.6 Stage 1 Engineering Concept

The engineering CAD model of the laser-driven ion source is in progress; the present concept is shown in figure 15. Though no decisions have been made on suppliers of equipment at this stage of the project, the CAD model representation of the 100 TW Ti:S laser and pulse-compressor chamber has been provided by the company "Amplitude". The laser equipment is shown supported by 2 optical tables, support modules M1 and M2, followed by a compressor chamber, module M3. Figure 16 shows a provisional representation of the target chamber internal components. The conceptual design will be developed over the next 18 months. Modules M4 – M9 are independent support systems which will be assembled, surveyed and tested prior to installation in the accelerator complex. Power supply, control and instrumentation racks will also be cabled to the modules in the pre-installation assembly area to test the racks and control-system elements. This proven methodology will
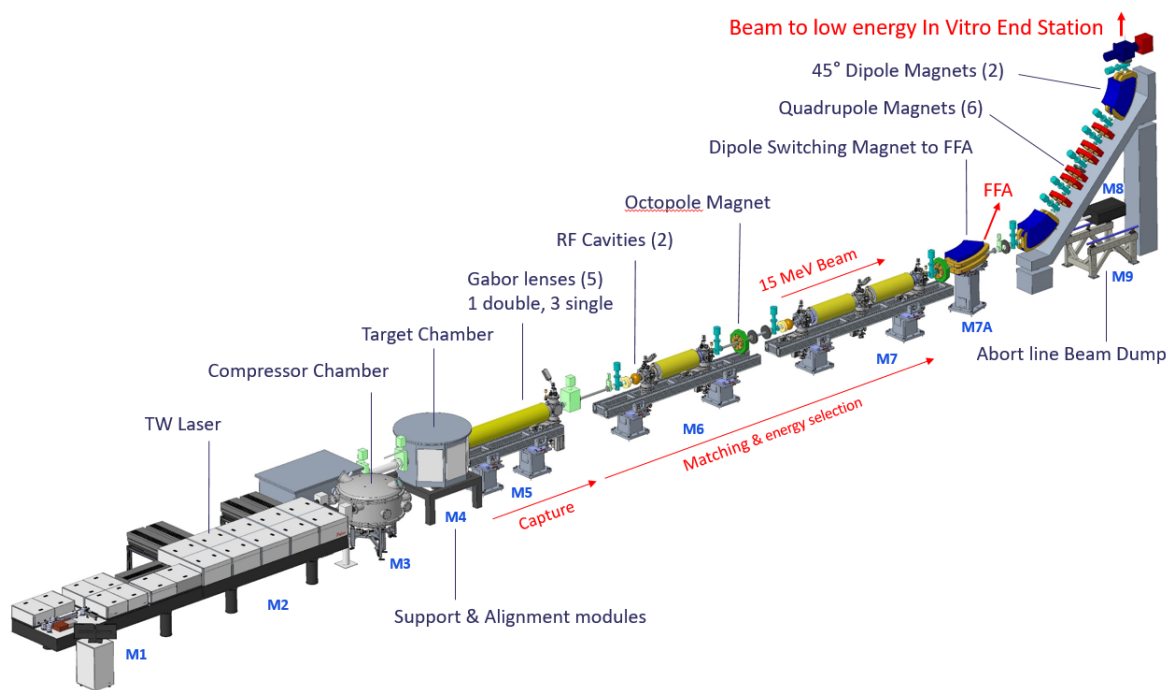
Figure 15: Stage 1 engineering concept design.

be used to solve as many technical issues as possible prior to installation, thus reducing the time required for installation and commissioning. Support-, alignment- and vacuum-system design is based on previous UKRI–STFC facilities. Module M8 is a representation of the $45°$ girder assembly. Permanently installed working platforms next to module M8 are envisaged to provide safe and efficient working at height. Internal craneage will also be required in some areas.

1.6.2.7 Schematic Diagram

A draft schematic diagram of the facility is shown in figure 17. A large format version with clearer visualisation of the required components is available [48]. A draft device naming convention has been established [49]. The device naming convention has the following benefits:

- Every device on the facility has a unique name;
- Names are used in an appropriate and consistent way;
- Duplicate names can be avoided;
- The function of a device can be derived from its name (and vice versa); and
- Consistency with good practice adopted on previous accelerators constructed and operated successfully.

It is proposed to introduce a formal device naming convention on the LhARA Control System. It is anticipated that the names will be used on the facility schematic, engineering drawings, in technical documents, control system display panels, and in informal and formal discussions. The plan is to develop the schematic throughout the Conceptual Design Phase to capture all the equipment required that will inform the CAD model, cost model and schedule.

24

Figure 16: Concept design of the Target, Conductance Nozzle and first Gabor lens.

Figure 17: Schematic diagram of the facility equipment.

Table 5: Envisaged mean working pressure for each vacuum region.

Subsystem	Mean working pressure (mbar)
Laser systems	TBC
Target chamber	1×10^{-6}
Gabor lenses	1×10^{-8}
Low energy line	1×10^{-8}
Low energy *in-vitro* end station	TBC
Fixed Field Accelerator	1×10^{-9}
High energy line	1×10^{-8}
High energy *in-vitro* end station	TBC
High energy *in-vivo* end station	TBC

1.6.2.8   Vacuum System

The vacuum system for the LhARA facility can be divided into a number of vacuum regions that require different vacuum specifications. The design presented below is based on the extensive experience of the design team in delivering successful vacuum systems for facilities such as Diamond Light Source at the STFC–Harwell Campus, and ALICE, EMMA and CLARA at UKRI–STFC Daresbury Laboratory.

The range of vacuum requirements falls comfortably in the ultra-high vacuum region. The Vacuum Quality Assurance Documents for modern accelerator applications developed at Daresbury Laboratory provide a good example of design principles that can be adopted for LhARA. As this project will involve a number of different partners it is essential that all vacuum systems, including those delivered by the partner institutes, are carefully integrated. This function has been identified and will be the role of a specific work package for integration of the whole project including vacuum systems. In addition, it is likely that it will be advantageous for the procurement of the vacuum equipment for the complete accelerator will be the responsibility of a single point of contact. Key vacuum challenges for LhARA include:

- Achieving low pressure without extensive in-situ bakeout;
- Maintaining a contamination-free environment, including some particle controls, particularly in the region of the RF cavities;
- Providing sufficient differential pumping where vacuum specifications vary by more than one order of magnitude between sections; and
- Providing sufficient pumping for conductance limited beam pipes.

General Design Objectives

In any accelerator-based project, it is inevitable that detailed consideration of the vacuum system comes some way down the line in the design process. The major reason for this is that a relatively detailed understanding of the mechanical layout of the machine and of the design of individual vacuum vessels and components is required before any final analysis of the pumping requirements can be made. At this stage in the LhARA design, more detailed engineering is required to finalise the conceptual design; this may result in some adjustments to the vacuum system but these are not expected to be significant. It is recommended that all components receive a full UHV cleaning followed by a vacuum bake to 250°C for 24 hours before installation (ex-situ) where possible. Differential pumping will be required to minimise gas and debris transfer between the laser target and the first Gabor lens; this will be studied during the modelling stage of the Conceptual Design before the 12 month design review.

Vacuum System Design Principles

General

In general, the vacuum system design of LhARA is not particularly demanding, except for the target-–Gabor lens differential pumping section. Knife-edge sealing is the default standard for bakeable vacuum systems of the type required for LhARA. However, in recent times, the reliability of EVAC seals has been proven on a number of machines and it may be that their compact size could be an advantage in some areas; their use will be considered during the technical design stage of the project. To ensure that all vacuum equipment is compatible with each region of the accelerator complex it is important that flange connections are clearly specified. Unless otherwise stated, all vacuum equipment will use the ConFlat$^{\text{TM}}$ Flange (CF) standard to connect to the vacuum system. This is the most common type of flange connection for ultra-high vacuum systems and uses the knife-edge principle to achieve an all-metal vacuum seal.

Vacuum Pumping

It is expected that the LhARA vacuum system will be conductance limited in most places. This will limit the pressures that can be achieved using a reasonable number of pumps. As usual, a number of iterations of machine layout and calculation of pressure distributions will be required before a satisfactory final vacuum-pumping scheme can be determined. At this stage an estimate has been made based upon previous experience. Since the whole machine is sensitive to hydrocarbon contamination to a greater or lesser degree, rough pumping will not use any oil-sealed pumps. Pre-pumping will use scroll pumps for a good balance of pumping throughput and cost. The high vacuum pumping will use clean turbomolecular pumps. These pump sets will be mounted on roughing carts that can be moved into position when required. Main UHV pumping will be by sputter ion pumps, supplemented by NEG cartridge pumps if required in critical areas. The ion pump power supplies will be located in rack rooms outside the accelerator complex. To reduce costs, power supplies with multiple outlets will be used. The disadvantage of this approach is that the pressure indication for each individual pump is compromised such that it cannot be relied upon as a true indication of pressure. However, this approach reduces costs significantly and has been used successfully elsewhere.

Pressure Measurement

Adequate pressure-measurement performance will be obtained using Pirani Gauges and Inverted Magnetron Gauges supplemented by information from ion pump power supplies and residual-gas analysers (RGAs). RGAs will be placed at a few strategic locations throughout the accelerator complex. Otherwise, RGA facilities will be mounted on the mobile roughing carts where they will be used mainly for leak testing and monitoring of initial cleanliness of the systems. The total-pressure-gauge controllers will be located in the rack rooms outside of the accelerator complex, so long cables will be required to connect these to the gauge heads. The specification of cable for this purpose will need to consider the minimisation of noise and interference of gauge operation. For the residual gas analyser the main electronic unit will be located close to the analyser head but sufficiently decoupled (via an RF cable extender) to avoid unwanted radiation damage or high magnetic fields.

Valves

Gate valves are required to provide sectorisation of the complete LhARA vacuum system for practical reasons and for machine protection. Dividing the machine into discrete vacuum regions makes it easier to install and commission whilst simplifying maintenance and breakdown interventions. At the same time, it is important to keep the number of gate valves at a minimum to reduce costs. In most circumstances gate valves will be metal. Roughing valves (right-angled valves) and let-up valves will be located in each vacuum region. These will be

of an all-metal construction and for pump-down will be sized as DN63.

Bakeout

It is likely that most of the machine will not be baked in-situ, although all the vacuum chambers of the machine will be baked prior to installation as part of the conditioning and cleaning process unless there is a special component that cannot be baked. However, the system is designed such that in-situ bakeout may be used if necessary, e.g. to improve vacuum levels after interventions.

Vacuum Control System

A full system of vacuum controls will be installed on LhARA to provide monitoring, automation, alarms and safety protection.

1.6.2.9   Control System

In a complex facility such as LhARA, a unique control system will manage the whole machine, from the laser to the end stations. This means that the control system must be able to execute commands on all the active elements and control all the diagnostic devices and experiments, providing the required information to people operating the facility. Furthermore, it has to be easy to upgrade the system substituting old elements or introducing new ones. In general the main operations in an accelerator control system will be:

- data taking;
- display of information;
- data analysis;
- command execution;
- storage;
- automatic operation; and
- alarms management.

It is expected that the facility will use the Experimental Physics and Industrial Control System (EPICS) [50]. The logic and organisation of this system will be developed during the conceptual and technical design phases of the project, which will enable the accelerator design and end stations to progress with a full understanding of what types of instrumentation and control will be required.

1.6.2.10   Electrical Engineering

Electrical Equipment and Services

There are three rack rooms positioned around the accelerator, each capable of housing 20 standard racks. This even distribution of racks and the numerous local labyrinths minimises cable lengths, improves energy efficiency and simplifies installation. The location of some equipment is restricted by cable length, such as motion control and laser auxiliaries, so their position will need to be allocated accordingly. The labyrinth design should consider cable routes inside the accelerator and ensure personnel access is not affected. A possible alternative is high-level cable management. The energy efficiency of the power converters will dictate the rack layout and the heat loading within the rooms. The performance of the magnet power converters has not been assessed, but it is assumed that the required stability, reproducibility and resolution can be achievable using standard commercially-available units. The extraction system does need to be assessed to gain a better understanding of the proposed solution, as a pulsed system will create challenges given the ion energy and the envisaged

extraction angle.

Electrical Distribution

Currently the facility is envisaged to be supplied by a single transformer. Although this will be rated to provide the total estimated power consumption it is not ideal for continuity of supply. Additional considerations need to be assessed such as fault analysis and maintenance, along with segregation of supplies and conducted harmonics. It is important to design the electrical infrastructure to mitigate these factors, for example by increasing the number of transformers to offer a minimum "$n + 1$" redundancy or, alternatively, ensuring that there are dual HV supplies via a ring main unit to feed the local transformer. This philosophy should be cascaded throughout the LV distribution to ensure the failure of one circuit does not result in prolonged periods of downtime.

The facility will consist of numerous non-sinusoidal loads, such as DC magnet power converters, RF modulators and ion-pump power supplies. The harmonic currents generated from this equipment can have an adverse effect on other equipment connected to the distribution system. Ideally these issues will be dealt with at the equipment level, but this is often overlooked due to the cumulative effect of many devices connected to the same network. Wherever the facility is built, existing harmonic levels will need to be measured and included in any calculations to ensure compliance with legislation.

Segregation of the mains supply is important to ensure the required experimental performance is achieved, as some equipment will cause electrical disturbance, due to harmonics, sudden changes in demand and in-rush currents. The point of common coupling between these systems and the sensitive equipment becomes critical and will be considered when designing the electrical infrastructure.

Earthing Arrangements

The earthing (or grounding) scheme proposed for this facility must guarantee personal safety and the correct operation of power converters, vacuum systems, diagnostics instruments and motion-control equipment. It must also ensure compliance with safety and EMC requirements from applicable standards. The primary goal of an earthing system is to assure personnel safety and protection of installations against damage. Two critical phenomena are lightning and power-system faults. These can cause circulation of large currents, which might create hazardous voltages in installed structures. In these conditions, the earthing system is to be a path to earth for currents, while maintaining minimum voltage differences between any two points of the installation. The secondary requirement of an earthing system is to serve as a common voltage reference and to contribute to the mitigation of electrical disturbances in installations with sensitive and interconnected electronic and electrical systems. This facility is expected to generate conducted noise at the following frequencies:

- Mains frequency (50 Hz) and multiples of this frequency due to non-linear loads, which make use of uncontrolled rectifiers to convert AC-DC. There are many examples of sources of noise at these frequencies these include:
    - All devices that contain a switch mode power supply;
    - Uninterruptible power supplies; and
    - Inverters for AC motors/pumps;
- High frequency (1 kHz to 100 kHz): coming mainly from magnet power converters, and RF system capacitor chargers, due to switching within the converter.

Radiated noise is also expected throughout the RF spectrum emanating from some of the equipment below:

- Pulsed magnet power supplies for kickers and septum magnets;
- Pulsed power supplies for RF amplifiers such Klystrons; and
- Mobile phones and Wi-Fi signals are common and required across much of the Daresbury site and the associated frequencies also represent a source of radiated noise.

It must also be acknowledged that some specialist experimental equipment may not comply with electro-magnetic immunity or susceptibility standards. This may be due to method of operation or the technology readiness level of the device. Detailed investigation of this equipment and the method of operation must be made to ensure this equipment does not have a detrimental impact on other local systems, and may require the incorporation of specialist noise-reduction techniques. Best practice for these types of facilities is to install two grounding networks, a safety grounding network and reference grounding network, bonded together. Their design and interconnection will depend on the layout of the accelerator and support areas, such as rack rooms and RF equipment.

1.6.2.11 Key Events

Date	Event
13/01/2022	UKRI Ion Therapy Research Facility Webinar Document: UK Ion Therapy Research Facility Webinar - Agenda 130122 \\fed.cclrc.ac.uk\org\NLab\ASTeC-TDL\Projects\tdl-1272 ITRF\pa1 - CDR\bid - Business Innovation Directorate
26/01/2022	ITRF Advisory Committee Meeting #4
27/04/2022	LhARA Collaboration Meeting
28/04/2022	Future accelerators for biomedical applications Workshop
18/05/2022	ITRF Advisory Committee Meeting #5
13/06/2022	CERN – UKRI STFC Framework Collaboration Agreement KN 5444/ATS signed
20/07/2022	ITRF Advisory Committee Meeting #6
28/9/2022	ITRF IF monitoring Kick Off Meeting
01/10/2022	ITRF Project Start
14/10/2022	LhARA collaboration meeting. Schedule of presentations and agenda at `https://indico.stfc.ac.uk/event/628/`
19/10/2022	ITRF STFC press release `https://www.ukri.org/news/researching-a-new-generation-of-technology-to-treat-cancer/`
26/10/2022	LhARA/ITRF international review `https://ccap.hep.ph.ic.ac.uk/trac/wiki/Research/DesignStudy/Reviews/AugSep22/Review/29-30Sep22`
03/11/2022	ITRF Advisory Committee Meeting #7
07/11/2022	ITRF Project Board meeting #1
29/11/2023	LhARA/ITRF international review Feedback. Document LhARA-Gov-Rev-2022-01 `https://ccap.hep.ph.ic.ac.uk/trac/wiki/Research/LhARA/Documentation/TN/Governance` Document reviewed: LhARA R&D proposal for the preliminary, pre-construction phases. CCAP-TN-10.
01/12/2022	ITRF JeS grants approved
05/12/2022	Request to UKRI to re-profile finance
14/12/2022	Novel End Station Consultation Meeting `https://indico.stfc.ac.uk/event/668/` Baseline document: LhARA-Gov-PMB-2022-01
18/01/2023	Infrastructure Fund Project Catch-up - Ion Therapy Research Facility
01/02/2023	Ion Therapy Research Facility updated award letter received via J A Clarke by e-mail
08/02/2023	LhARA Collaboration meeting #3 Vinen Room in Physics West, School of Physics and Astronomy, Birmingham, B15 2TT `https://indico.stfc.ac.uk/event/685/`
12/03/2023	LhARA collaboration response to international review of LhARA, document LhARA-Gov-PMB-2022-02
21/03/2023	ITRF 6 month Design Review `https://indico.stfc.ac.uk/event/722/`
23/03/2023	ITRF Project Board Meeting #2

1.6.3 Work towards updating the lattice design

Simulation efforts use a number of software packages. MADX [51] and BeamOptics [52] are used for rapid initial design and modification assessment by modelling the transport of the beam envelope when not considering space-charge forces. GPT [53] is a Monte Carlo tracking code that can model space charge effects and is used for evaluating beam transport performance and optimisation. Finally, BDSIM [54] is another Monte Carlo
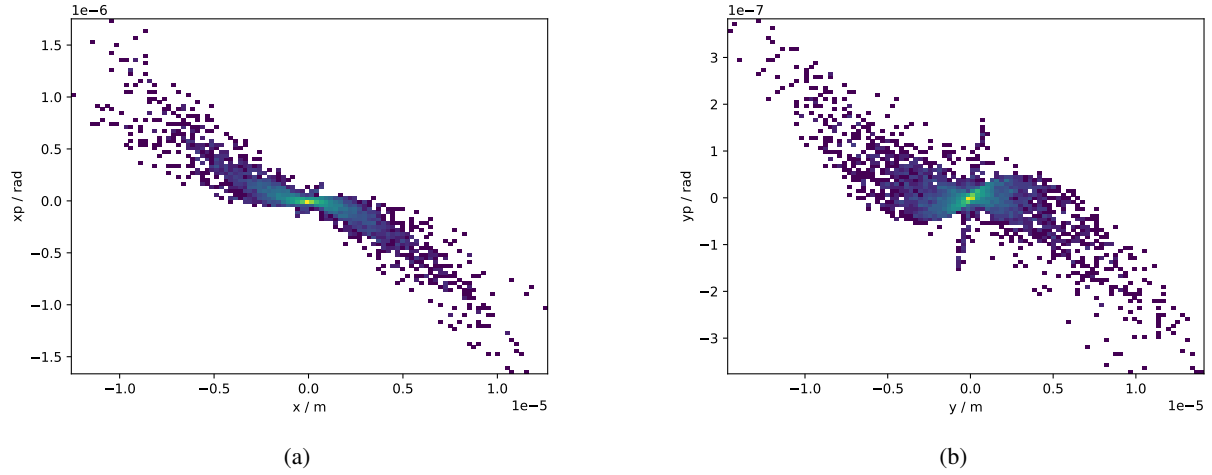
Figure 18: Phase space residuals at the stage 1 end station with the first octupole on minus off.

particle-tracking tool based upon Geant4 and is capable of modelling particle-matter interactions. BDSIM is used for further transport performance evaluation, including collimation, particle loss estimation, and energy deposition studies.

1.6.3.1 Recommended baseline changes

The baseline design [41] contains two octupoles by which to generate a uniform spatial distribution of the beam at the end station. The first of these is located close to the focal plane of the third Gabor lens where the beam radius is at a minimum, therefore its impact is anticipated to be minimal. Figure 18 shows the phase-space difference at the Stage 1 low-energy *in-vitro* end station when the octupole is on minus that when the octupole field is zero. This was modelled in BDSIM for the baseline configuration which delivers a 1.2 cm radius (at 1σ) beam to the end station. The phase-space residuals show a maximum difference several orders of magnitude smaller than that of the beam dimensions, strongly indicating that the octupole is having minimal effect. It is therefore recommended that this magnet be removed from the Stage 1 beam line. Octupoles remain the primary choice for producing uniform beams and the placement of a second octupole in an optimal location will be investigated in future work.

The baseline design requires Stage 1 to produce a beam with Twiss functions of $\beta_{x,y} = 50$ m, $\alpha_{x,y} = 0$, and $D_{x,y} = 0$ at the end of the matching section for transport through the FFA injection line. To meet these requirements, the Gabor lens strengths must be modified, notably the third lens which focuses the beam for energy collimation. However, this change also modifies the lens focal length and consequently the energy collimator will not perform as efficiently as desired. Therefore, a second collimator has been added 20 cm downstream of the first collimator, at the focal plane of the third Gabor lens in the FFA injection configuration. The collimator aperture has provisionally been chosen to be identical to that of the first collimator; however, further studies will optimise the aperture to provide the desired energy spread at the end station. Figure 19 shows the recommended updates to the Stage 1 baseline.
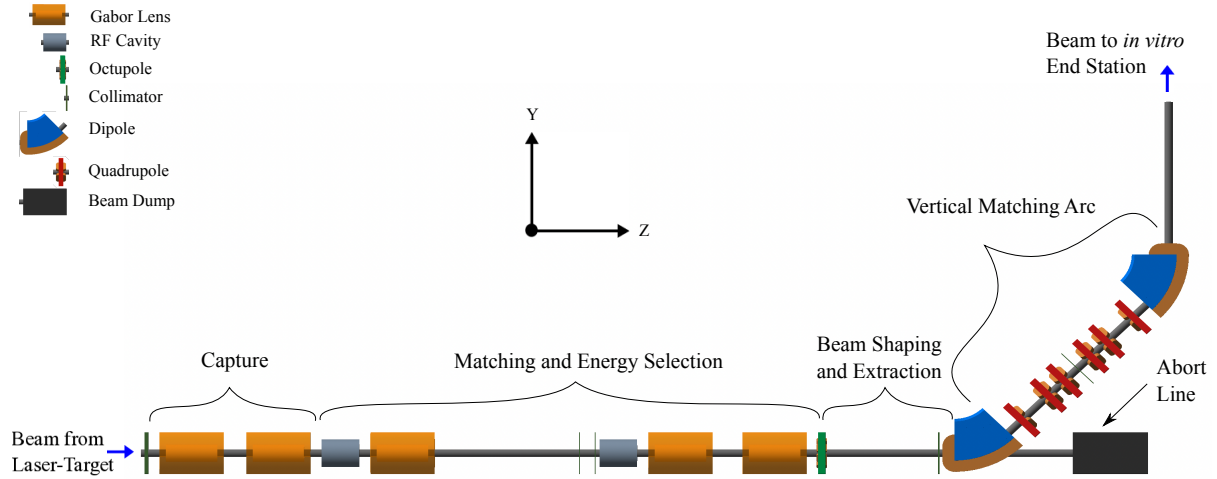
Figure 19: Schematic diagram of LhARA Stage 1 beam transport with recommended baseline updates.

1.6.3.2 Beam Parameters

Modelling of the first 10 cm of beam transport after the target maintains our previous methodology. The beam is down-sampled and filtered to limit its spectrum to 15 MeV ± 2%. The beam is tracked for 5 cm without space-charge forces, maintaining our assumption that the proton and electron beams generated by the laser-target interaction co-propagate over this distance. A 2 mm transverse radial cut is applied approximating propagation through the vacuum nozzle entrance aperture. The beam is then tracked for 5 cm with space charge forces being modelled, assuming a total bunch charge of 1×10^9 protons, after which a second radial cut of 2.87 mm is applied representing the nozzle exit aperture.

A tracking code is used to transport a particle beam generated from the output of the simulation of the laser-target interaction. The particle-in-cell (PIC) code SMILEI [55] was used in the preparation of the pre-CDR [3]. Although being the best available simulation effort at the time, the code constrained the modelling to two spatial dimensions, with the third dimension (vertical axis) being assumed to have a similar kinematic distribution to that of the simulated horizontal axis [56]. When comparing the beam parameters to the assumed values used in the pre-CDR design [3], a difference of approximately an order of magnitude was observed in the emittance, as outlined in table 6. At present it is not fully understood why such a discrepancy is seen; however, 2D TNSA simulations are known to suffer from several issues [56]. Consequently the current SMILEI simulation data is now not considered to provide a reliable description of the LhARA beam.

	Pre-CDR Beam	SMILEI Sampled Beam	SCAPA Sampled Beam
Mean RMS Emittance [m]	3.26×10^{-7}	1.43×10^{-8}	7.98×10^{-8}
Mean Beta [m]	4.89	141.34	21.62
Mean Alpha	-50.22	-1418.43	-222.23

Table 6: Beam parameters at the exit of the target housing.

An alternative beam description has been developed in LhARA Work Package 2 using the PIC code OSIRIS [57] to model the TNSA mechanism to produce a full 6D phase-space description of the accelerated protons. The new simulations use the laser parameters delivered by the SCAPA facility. The proton-beam parameters
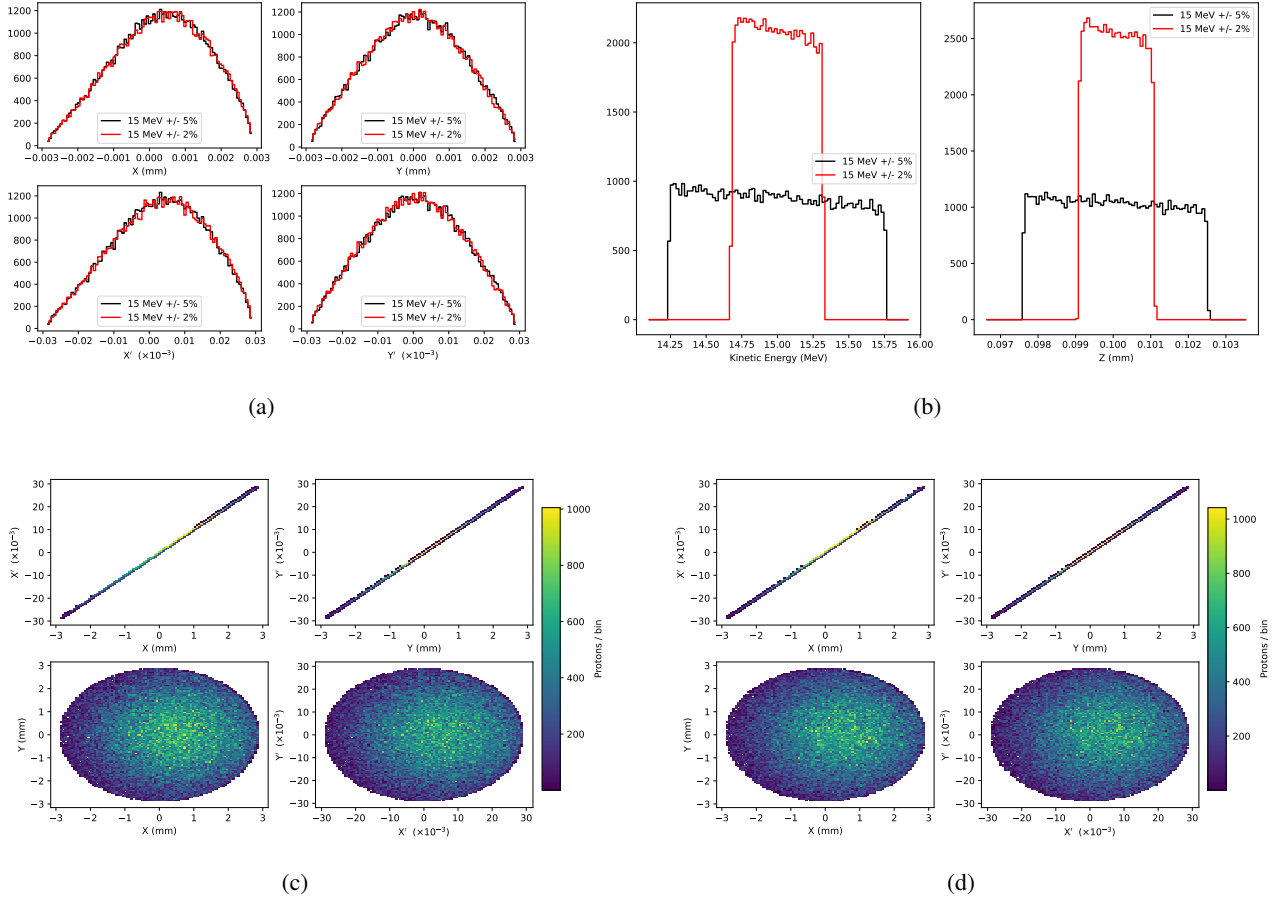
Figure 20: SCAPA beam profiles and phase space distributions for 15 MeV ± 2% and 5% beams.

produced using OSIRIS, listed in table 6, are significantly closer to those assumed in the pre-CDR. Although an approximate factor of 4 difference remains, we believe this distribution to be a more accurate representation of the phase space produced at the source. Recent simulation efforts have therefore tracked the distribution sampled from that produced using OSIRIS using the SCAPA parameters (referred to as the SCAPA beam in the paragraphs that follow).

To study the effect of the collimation system, a second beam was sampled to produce a spectrum centred on 15 MeV with a 5% spread. The phase spaces of both beams are shown in figure 20. In figure 20(a), the beams exhibit a horizontal offset in both spatial and momentum dimensions which is not fully understood at this stage; however, subsequent tracking to the end station shows that this offset does not impact beam-transport performance. The transmitted spectrum in figure 20(b) remains approximately uniform, matching the spectrum generated at the target despite being collimated by the vacuum nozzle. The longitudinal distribution in z shows a similar form to the energy distribution, as would be expected. Figures 20(c) and 20(d) show the full transverse phases spaces for the 15 MeV ± 2% and 15 MeV ± 5% beams respectively. Both beams show a highly divergent, circular beam as anticipated, indicating that the nozzle exit aperture strongly influences the beam shape and size. Further studies will establish the broader transmitted spectra to ascertain the nozzle performance and estimate losses within the capture section. This is necessary for both the Gabor lens mode of operation—the performance of which may be impacted by off-energy protons interacting with the lens' electron cloud—as well as the solenoid-based alternative where significant energy may be deposited within the magnets.

34

Table 7: Nozzle proton transmission efficiency.

Beam Energy (MeV)	Initial Distribution	Nozzle Entrance (with 2.00mm cut)	Nozzle Exit (with 2.87mm cut)	Nozzle Transmission (%)
$15 \pm 2\%$	100000	88709	69162	**76.70**
$15 \pm 5\%$	100000	88704	68044	**77.97**

The nozzle transmission efficiency, listed in table 7, shows similar performance for both $15\,\text{GeV} \pm 2\%$ and $15\,\text{GeV} \pm 5\%$ beams, with approximately half of particle losses occurring within the nozzle itself. As the current nozzle apertures do not impact the transmitted energy spread, in the future emphasis will be placed on establishing the downstream collimator performance.

1.6.3.3 Baseline Performance with the SCAPA Beam

The evolution of the SCAPA beam size along the Stage 1 beam transport sections is shown in figure 21 when space charge is considered and compared to the performance with out space charge. As observed in previous simulations, the emittance growth observed within the vacuum nozzle continues in the first 15 cm drift space after the exit flange. This space continues to be reserved to accommodate the physical length of the Gabor lens which is longer than the effective field length that is presently modelled as an equivalent solenoid. This emittance growth immediately impacts tracking performance, resulting in a divergent beam exiting the matching section prior to the vertical arc. A divergent beam is also observed after the capture section; a parallel beam is necessary in this location as the distance between the second and third Gabor lenses will require to be modified to accommodate diagnostic instruments, Gabor lens electron-injection systems, and the target-room shielding wall seen in figure 13. The exact length required of this drift is currently unknown; however, the flexibility yielded by a parallel beam permits the length to be determined at a later date. The beam waist after Gabor lens 3 is not at the desired location of the Stage 1 energy collimator; consequently the energy selection will not be performed with optimal efficiency.

Optimisation studies have been conducted to mitigate the space-charge-induced effects seen in figure 21. A GPT utility optimisation program, GDFSOLVE, is a multidimensional Newton-Raphson solver that has been used to optimise the strength of the 5 solenoids that represent the Gabor lenses. Initial optimisation aimed to reproduce the nominal beam size at the end of the matching section with a maximum solenoid field-strength of 1.4 T. The nominal and optimised solenoid field strengths, and the equivalent Gabor lens parameters, are listed in table 8. A solution was found in which, unusually, the first field strength was slightly below the 1.4 T constraint. This first focusing element is crucial for capture performance and strongly constrains the beam size after the second Gabor lens. It is believed that a solution exists where the first solenoid field is fixed at 1.4 T, however the impact on beam size is anticipated to be minor in such a scenario.

The optics of the optimised baseline beam transport are shown in figure 22. Here, all three objectives have been achieved: the beam is parallel after the capture section, the beam waist after Gabor lens 3 is at the location of the Stage 1 energy collimator, and the beam is parallel after the matching section. The beam radius of 12.99 mm in the capture section is the largest at any point along the Stage 1 beam-transport line. This size is ultimately determined by the aforementioned strength of the first focusing element but is also constrained by the exit aperture of the vacuum nozzle. Concerns remain about potential interaction between the tails of the transverse distribution and the Gabor lens' electron cloud. Calculation of the Gabor lens field voltages have assumed a cathode radius of 3.65 cm; however, the true radius of the electron cloud—which at present remains
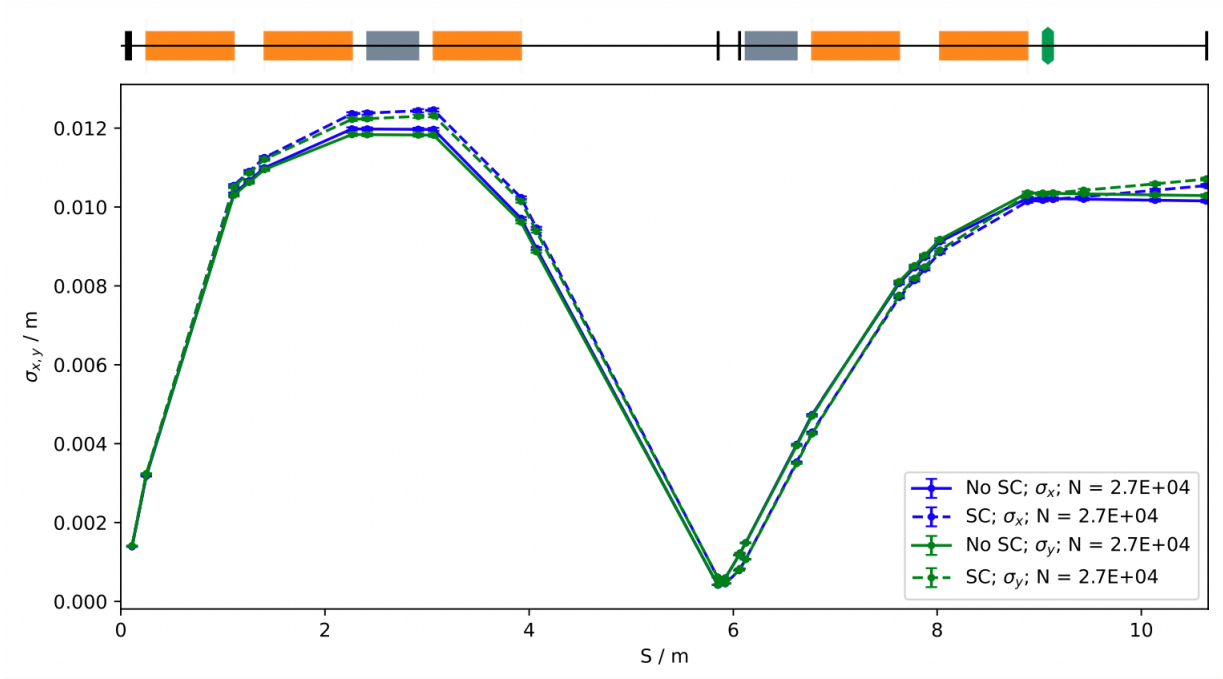
Figure 21: Stage 1 optics with and without space charge forces modelled for baseline solenoid settings.

Table 8: Nominal and optimised parameters of the five Stage 1 solenoids and equivalent Gabor lens parameters.

	Nominal			Optimised		
	Solenoid	Gabor Lens		Solenoid	Gabor Lens	
	Field (T)	e^- Density ($\times 10^{15}$)	Voltage (kV)	Field (T)	e^- Density ($\times 10^{15}$)	Voltage (kV)
GL1	1.438715	5.479	33.018	1.391631	5.126	30.892
GL2	0.527115	0.735	4.432	0.591842	0.927	5.587
GL3	0.813923	1.753	10.567	0.816040	1.763	10.622
GL4	0.728404	1.404	8.463	0.839703	1.866	11.247
GL5	0.633802	1.063	6.407	0.572477	0.867	5.227
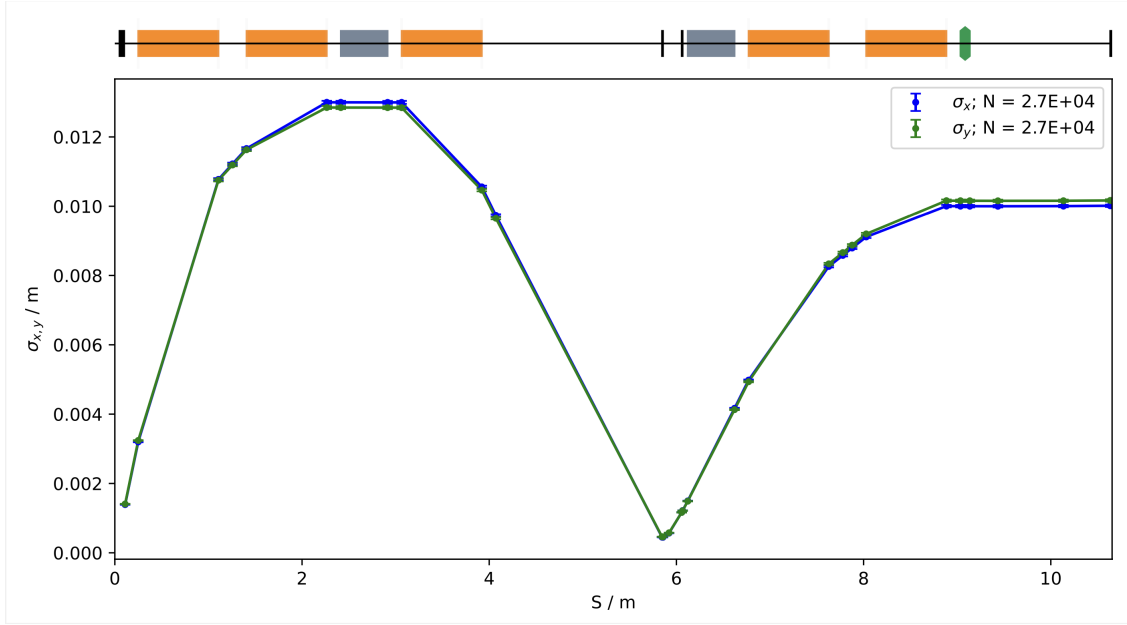
Figure 22: Optimised optics of the Stage 1 beam transport line.

Beam radius	9.0 mm	8.0 mm
GL4	1.027919	0.940095
GL5	0.953825	0.489305

Table 9: Optimised strengths of the 4th and 5th solenoids for delivering alternative beam spot sizes to the stage end station.

unknown and is to be experimentally determined—is likely to differ from the assumed value. This potential interaction must remain a consideration in ongoing efforts until more accurate information on the electron cloud is available.

Beyond the nominal configuration, additional solenoid-strength configurations have been found to demonstrate the intended flexible spot sizes that LhARA will deliver. Only the 4th and 5th focusing-element strengths were varied to preserve the performance of the capture section and the focal length of the third Gabor lens. The solenoid field strengths are listed in table 9.

To meet the performance requirement for injection into the FFA, the beam at the end of the matching section must have $\beta = 50$ m, given the emittance in table 6, this corresponds to a spot size of 2 mm. Solutions that deliver these parameters have yet to be found for both the nominal beam parameters and in the case when space-charge effects are considered. Work towards finding the required solutions is ongoing. Studies are also underway to find settings that deliver the range of spot sizes required.

1.6.3.4 7 Gabor Lens Configuration

To address the challenges encountered with the baseline design, a configuration containing seven Gabor lenses is being investigated. Presently, only the beam transport performance of this configuration is being considered; the necessary infrastructure modifications will be investigated in future work. The geometrical changes to the beam line are an increased drift length between Gabor lens 4 and Gabor lens 5 from 0.1 m to 0.3 m, an
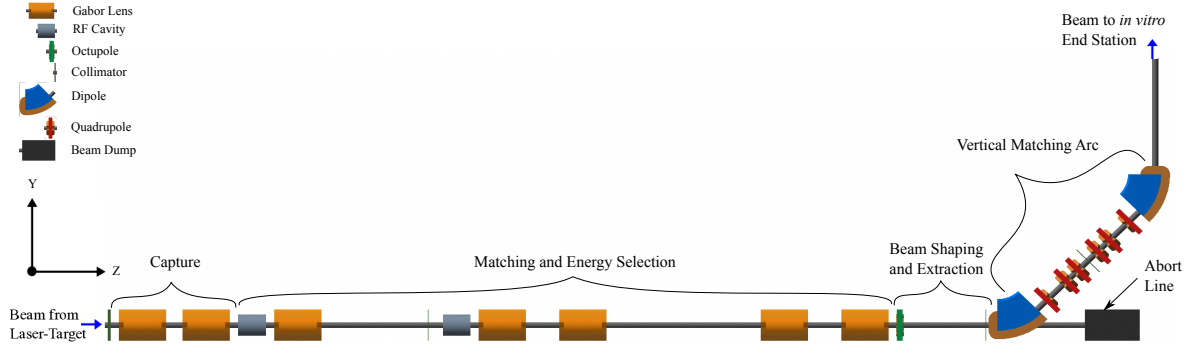
37

Figure 23: Schematic diagram of LhARA Stage 1 beam transport for the 7 Gabor Lens configuration.
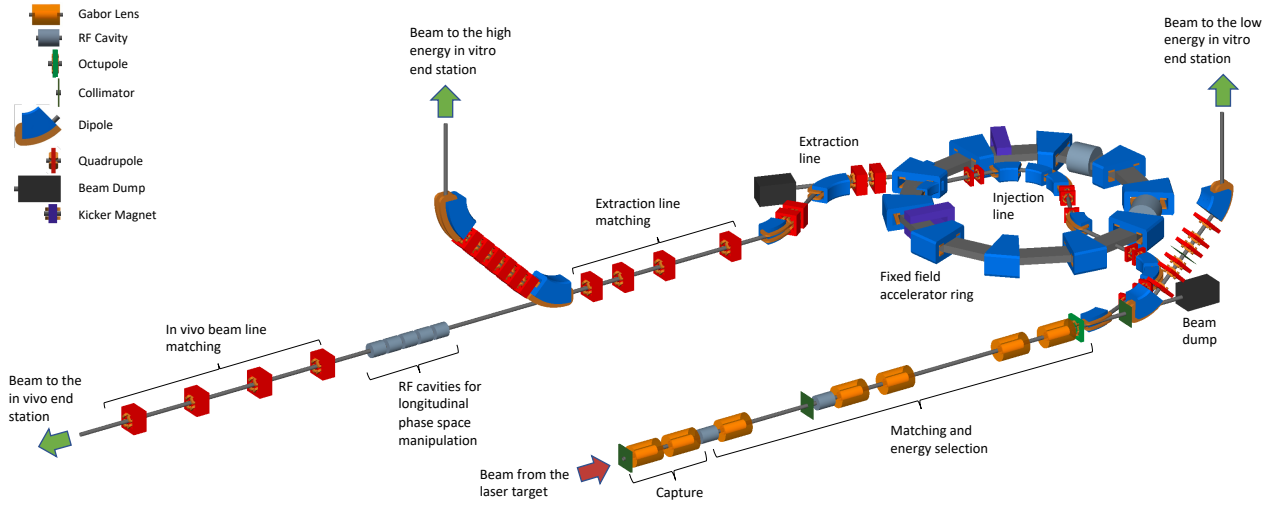

Figure 24: Schematic diagram of LhARA Stage 1 and 2 for the Gabor Lens configuration.

additional 2.5 m drift added downstream of Gabor lens 5, and the addition of two new Gabor lenses in the same configuration as the fourth and fifth lenses, including the 0.3 m distance between them. The overall length increase of Stage 1 is 5.314 m. A schematic diagram of the modified Stage 1 beam line is shown in figure 23.

A schematic diagram of both LhARA stages from the BDSIM model is shown in figure 24. Cosmetic changes to the BDSIM model to represent more accurately the geometry of the FFA have also been made in the figure. The FFA is not presently modelled in BDSIM in tracking studies.

In this 7 Gabor lens configuration, the capture section has been re-matched based upon the SCAPA beam parameters listed in table 6. A number of solutions have been found varying only in the strength of the downstream Gabor lenses in the matching section; consequently the first three Gabor lenses are not varied for any optical settings configuration that has been simulated. These Gabor lens strengths and the equivalent solenoid fields are listed in table 10. The constant strength of the third Gabor lens results in its focal plane being in the same location for both Stage 1 and Stage 2 operation. Consequently, this beam line configuration requires only a single energy collimator at 5.752 m from the exit of the nozzle (z=5.852 m from the target). The second energy collimator is replaced with the equivalent length of drift tube.

When not considering space-charge effects, a number of optical solutions have been found that yield a range of spot sizes at the Stage 1 end station. The strengths of the equivalent solenoid field for each solution is listed in table 11. Notably, a solution has been found that produces a beam that meets the conditions for transport

38

Table 10: Strength parameters of the first 3 Gabor lenses in the 7 Gabor lens configuration and their solenoid equivalent fields.

	Solenoid	Gabor Lens	
	Field (T)	e^- Density ($\times 10^{15}$)	Voltage (kV)
GL1	1.4000	5.188	31.265
GL2	0.5724	0.867	5.226
GL3	0.8139	1.753	10.566

Table 11: Matching solutions equivalent solenoidal field strengths for the 7 Gabor lens configuration.

Beta Value (m)	Beam size at the end station (mm)	GL4	GL5	GL6	GL7
704.89	7.5	1.0051	0.9014	0.6994	0.6551
489.51	6.25	1.0051	0.8647	0.7377	0.7106
313.28	5.0	1.0051	0.8247	0.7947	0.7984
176.22	3.75	1.0051	0.7715	0.8040	0.9829
78.32	2.5	0.9060	0.8018	0.2661	1.2793
50.0	2.0	1.1875	0.5833	1.4000	0.3982

through the FFA injection line. The sixth lens is at its maximum strength, indicating that smaller beams will be challenging to achieve should they be desired.

Figure 25 shows the beam size tracked in the GPT model without space charge forces compared to a nominal MADX model for the 7.5 mm spot-size optics settings. Only the sections of the beam line that have changed geometrically have been simulated. A small discrepancy between the two models can be seen which can be attributed to the non-Gaussian beam profile, seen in figure 20(a), being tracked in GPT.

When modelling space-charge forces in GPT, an emittance growth is observed in the capture section which affects the performance of the downstream optics, see in figure 26. Optimisation is required to meet three objectives: parallel beams at the end of the capture and matching sections; and the positioning of the focal plane of the third Gabor lens must be at the energy collimator.

Figure 27 shows the optimised settings for the 7.5 mm spot size configuration. The full Stage 1 beam line is simulated to assess the beam delivered to the end station. The beam leaving the vertical arc is slightly divergent as a consequence of slightly relaxed optimisation constraints; we are confident that a parallel beam can be achieved with minor tweaking of the strengths of the final 4 Gabor lenses. The optimised Gabor lens parameters and the equivalent solenoid field strengths are listed in table 12. The strengths of the first three lenses are identical for all settings and no further optimisation of these for beam transport performance evaluation is required at this stage.

Optimised solutions have also been found for 6.25 mm and 5.00 mm spot size settings identified in table 11. Just as in the case of the 7.5 mm spot size solution, minor tweaking is required. Solutions have yet to be found, however, for the smaller spot-size configurations. This remains the primary focus of ongoing work to demonstrate the intended flexibility of the model configuration.

Preliminary studies have been conducted to optimise the collimator settings to reduce the energy spread to 15 MeV $\pm$ 2% without significantly impacting the transmission efficiency. The Stage 1 beam line was simulated in BDSIM with the 15 MeV $\pm$ 2% beam, varying the aperture of the energy collimator. All other collimators
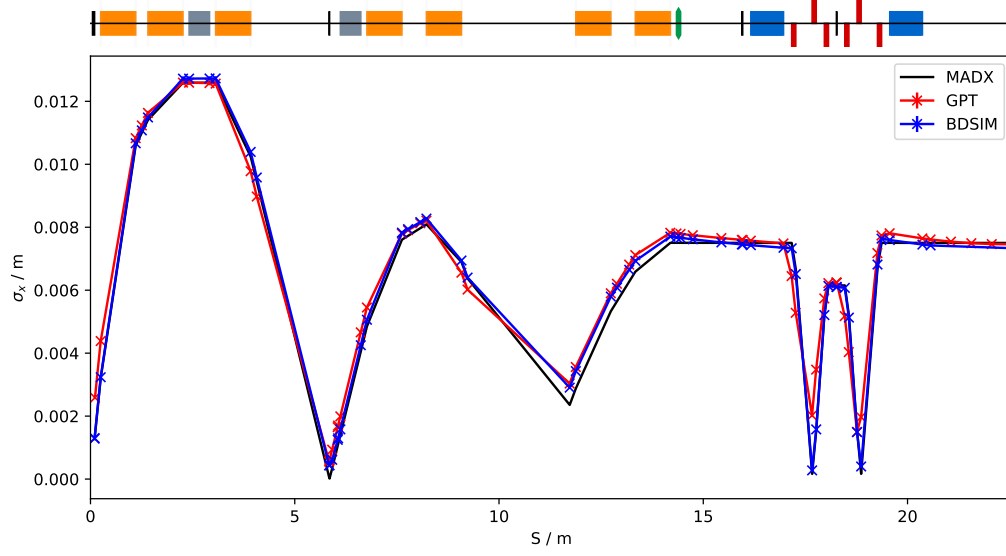
39

Figure 25: Validation of the GPT model of the 7 Gabor lens configuration against the nominal MADX design.
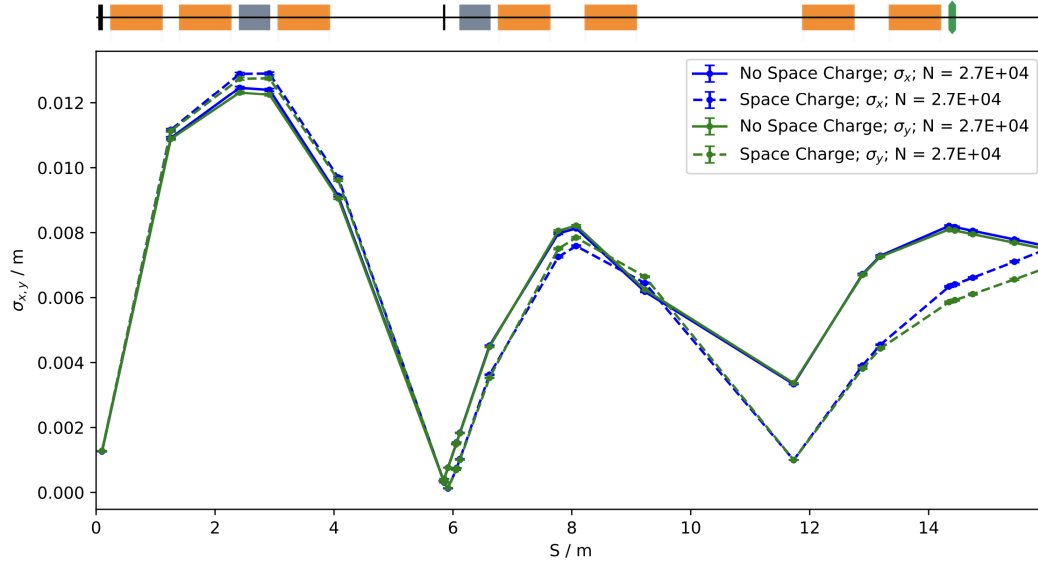

Figure 26: Impact of space-charge effects on nominal optical performance of the 7 Gabor lens configuration.
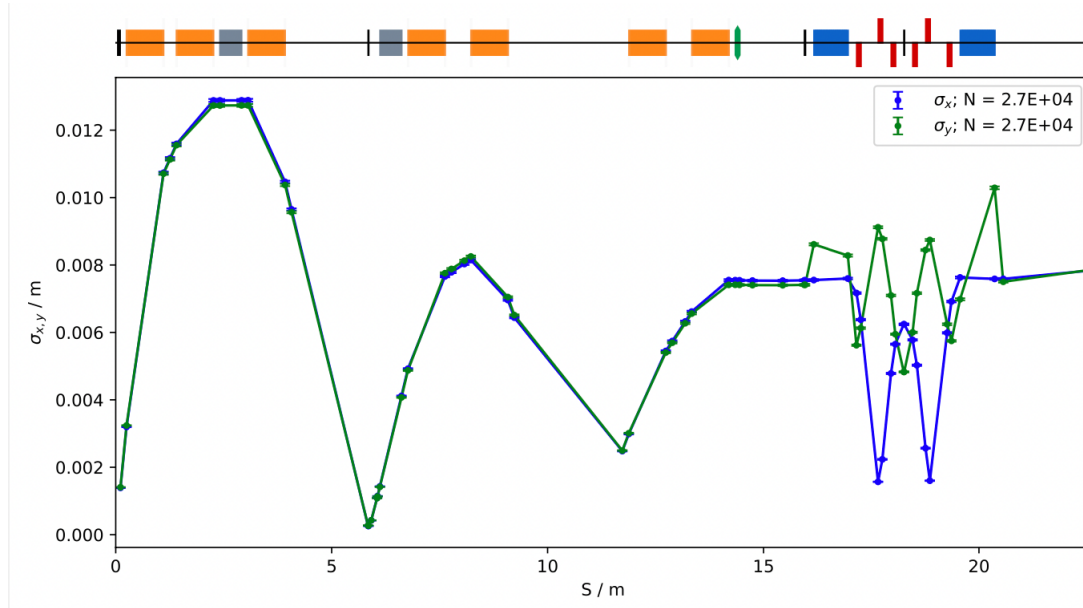
Figure 27: Optimised optics setting of the nominal 7 Gabor lens configuration.

Table 12: Optimised parameters of the 7 Stage 1 Gabor lenses parameters and solenoids equivalent fields.

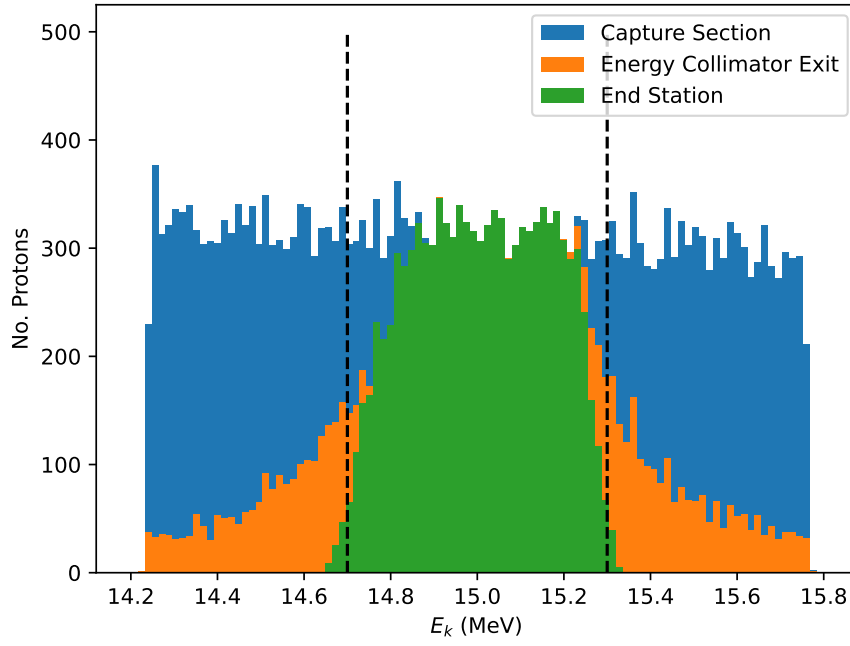| | Solenoid | Gabor Lens | |
	Field (T)	e^- Density ($\times 10^{15}$)	Voltage (kV)
GL1	1.4000	5.1880	31.267
GL2	0.582846	0.8991	5.418
GL3	0.817511	1.7689	10.660
GL4	1.007181	2.6849	16.181
GL5	0.903493	2.1606	13.021
GL6	0.733529	1.4242	8.583
GL7	0.642647	1.0931	6.587

Figure 28: Example energy spectrum recorded during preliminary studies of the energy collimator aperture settings. The black dashed line indicates the target energy cut-off of 15 MeV $\pm$ 2%.

remain unchanged from their nominal settings. Figure 28 shows the spectrum recorded at 3 locations for a circular collimator aperture radius of 1 cm: the end of the capture section (which is not expected to deviate from the spectrum transmitted from the vacuum nozzle); the exit of the energy collimator; and at the end station. The energy collimator clearly removes a significant fraction of the off-energy particles, however tails would clearly remain that extend beyond the $\pm$ 5% spread modelled. The spectrum at the end station is significantly improved, with only a small number of protons surviving beyond the 2% target. This indicates that the momentum cleaning collimator in the vertical arc contributes significantly to the energy selection performance. Therefore, another energy cleaning collimator is likely to be required in the FFA injection line for Stage 2 operation.

The transmission efficiency of the LhARA Stage 1 beam line for varying energy collimator aperture radius is shown in figure 29, along with the recorded beam size at the end station. The preliminary simulations indicate that apertures larger than $\approx$ 1 cm have little impact on the beam size, with only a modest drop in transmission over this range. Below 1 cm, the transmission begins to drop significantly whilst also reducing the beam size below the 7.5 mm target. The spectrum for the 1 cm aperture shown in figure 28 has a transmission efficiency of approximately 83%, indicating that the energy cleaning efforts are unlikely to have a significant impact on deliverable dose rates.

Currently, the 7 Gabor lens design is the main option for the next revision of the baseline.

1.6.4 RF

Acceleration in the FFA requires an RF system operating at a harmonic number $h = 1$, with an RF frequency range from 2.89 MHz to 6.48 MHz. Table 13 lists the key parameters of the RF system. Two technologies are being considered for the cavity: magnetic alloy (MA) loaded cavities; and ferrite-loaded cavities. The ferrite-
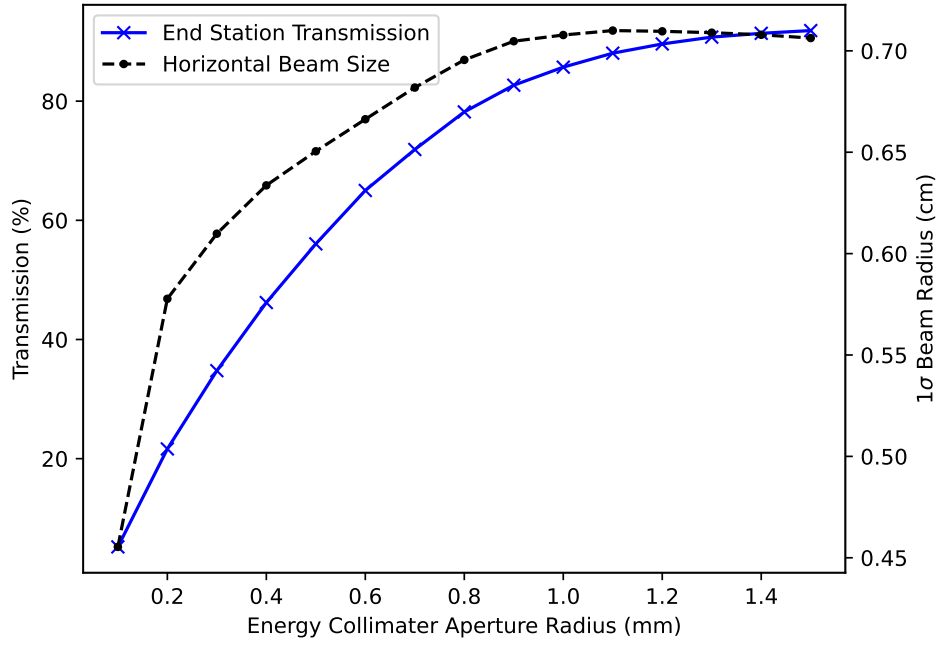
Figure 29: Preliminary calculations of transmission efficiency for varying energy collimator aperture sizes.

loaded cavity option requires a bias current (typically of the order of several hundred amperes) to modify the permeability of the ferrite cores through the acceleration cycle to obtain the required frequency variation. A typical configuration for a ferrite-loaded cavity uses two accelerating gaps per cavity to allow the same bias supply to drive the cores on either side of the gap. Thus, the space needed for a ferrite-loaded cavity would be more than that for an MA-loaded cavity. The MA-loaded cavity has a significantly higher bandwidth allowing the cavity to be driven directly with a variable frequency RF power supply, at the cost of higher losses and thus higher running costs. The arc length per cell determines the space available for the magnet and the cavity. This corresponds to a 2 m long section for the nominal ring radius of 3.2 m. In the baseline optics design, a drift space with a length of approximately 1.3 m remains once the length of the magnet is accounted. The cavity is required to fit in this space. Therefore, if the lattice of the FFA is not to be revised, the space constraint may be a critical issue for the choice of technology since the ferrite-loaded cavity is expected to be significantly larger than the MA-loaded cavity.

It will be important to establish through measurement that the performance of both core materials is capable of delivering the required accelerating gradient over the required frequency range. Work for the FETS FFA ring design at ISIS is underway, including the investigation of material properties for MA-loaded cavities and ferrite-loaded cavities. Since the required frequency range is similar to that needed for the LhARA FFA it is possible to use these results to realise a conceptual design for the RF system.

1.6.5 Next steps

Our methodology for beam transport in the first 10 cm after the target introduces an uncertainty into the performance of the LhARA beam transport. In additional to the SCAPA proton distribution that is being tracked, the recent SCAPA TNSA simulation output included phase space and spectral data on the electron distribution. The

Table 13: Summary of estimated parameters of the RF system of the FFA ring.

Parameter	unit	value
Proton RF frequency range	MHz	2.89–6.48
Harmonic number		1
Drift length per cell	m	1.3
Number of cavities		2
Estimated voltage per cavity	kV	4

Monte Carlo software capable of modelling space charge forces that we use (GPT, OPAL) cannot track beams composed of particles with differing charges. We are therefore planning to investigate alternative solutions that can solve the Vlasov equation for co-propagating beams, which remains a challenging research topic. This will greatly improve our understanding of the proton distribution at the exit of the nozzle, and consequently our confidence in the beam tracking performance of the LhARA accelerator.

Following the enhanced understanding of the behaviour of the co-propagating electron and proton beams, a study on the need to control the beam size in the capture section would be beneficial to determine the consequences of interaction between the Gabor lens electron cloud with the tails of the proton beam. Input from LhARA Work Package 3 on the estimated radius of the electron cloud in Gabor lens would aid this. The beam size is largely determined by the vacuum nozzle exit aperture. Reducing this aperture to achieve a reduction in beam size, should this be desired will negatively impact the transmission.

The 7 Gabor lens configuration currently being investigated is a promising candidate for a revised baseline configuration that has significant potential to deliver the intended Stage 1 spot-size flexibility. Going forward, work will continue on optimising of the spot-size optics and demonstrating the tracking of a beam suitable for transport through the FFA injection line.

Further intended Stage 1 studies include:

- Optimisation of collimator settings to yield beams with the correct energy spread whilst preserving beam size and maximising transmission;
- Identification of a suitable location for a second octupole and the optimisation of the octupole strengths required to deliver the intended lateral profile uniformity;
- Studies of loss maps and energy deposition to improve transmission understanding;
- Modelling RF cavities to determine performance in manipulating the longitudinal phase space distributions;
- Assessing optimal locations for correctors and non-transport related systems, such as diagnostics, vacuum ports, radiation shutters, etc. and incorporating these into our models;
- Assessing modifications necessary to accommodate infrastructure and safety requirements, particularly shielding walls;
- Studies of the lattice where Gabor lenses are replaced by solenoids and a Wien filter is added to perform ion-species selection. This lattice is a backup solution to mitigate the risk that the Gabor lenses can not be produced on an appropriate schedule; and the
- Investigation of alternative lattices in which the matching section, or the entire transport-line lattice, is based on quadrupoles.

The last six months saw little progress in the development of the design of the Stage 2 lattice. Several studies are foreseen in the near future, including:

- Updating the FFA lattice to incorporate the tunability required for variable energy extraction;
- Redesigning the injection line to allow for the shielding between the Stage 1 room and the FFA room;

44

- Optimisation studies with space charge;
- Conceptual design studies on the RF system;
- Conceptual design studies on the FFA magnet; and
- Assessing optimal locations for correctors and non-transport related systems, such as diagnostics, vacuum ports, radiation shutters, etc. and incorporating these into our models.

2 Work package 2: Facilities and costing

Over the reporting period, work in work package 2 has focused on the development of conceptual designs for the LhARA infrastructure. The work performed is summarised in section 1.6.

3 Work package 3: Conventional technology

ITRF WP3 aims to compare options based on conventional technologies against the novel approaches adopted as part of the baseline LhARA accelerator design [2]. This report describes work towards the preliminary design of a facility based on a room-temperature synchrotron, and an injector that uses established ion source technologies. We present key parameters and outline plans for future work on the synchrotron design.

3.1 Introduction

The scope of WP3 includes the conceptual design of a facility based around a slow-cycling ($\sim$1 Hz) room-temperature synchrotron, fed from an injector that uses established ion source technologies and pre-acceleration methods. This design study is intended to enable quantitative comparisons between a conventional accelerator and a facility entirely based on LhARA.

Here, we describe the current status of the WP3 synchrotron design study. In section 3.1 we state the requirements for the synchrotron design, and review similar designs proposed by the CERN NIMMS study. In section 3.2 we describe the preliminary design of a machine that meets these requirements. Section 3.3 gives an overview of the proposed injector parameters, while section 3.4 briefly outlines the main scheme for beam extraction, and section 3.5 provides estimates for the dose rates delivered to end stations from the synchrotron.

3.1.1 Synchrotron Requirements

The key requirements for the WP3 synchrotron design are as follows:
- **Choice of Ion Species**
  To maximise the usefulness of the synchrotron, its specifications have been chosen to accommodate ion species that are most likely to be used for radiotherapy. At present these are expected to be protons, helium and carbon ions [58].
- **Machine Parameters**
  To provide a direct comparison against the baseline LhARA design, the synchrotron should fit within the circumference of the LhARA FFA (21.86 m) and accommodate beam energies up to its nominal extraction energy. The extraction energy of the LhARA FFA for carbon ions is 33.4 MeV/u [2].
- **Beam Intensity**
  Ideally, the synchrotron should support beam intensities that are compatible with the delivery of FLASH dose rates to its end stations. The FLASH regime is generally defined as time-averaged dose rates of
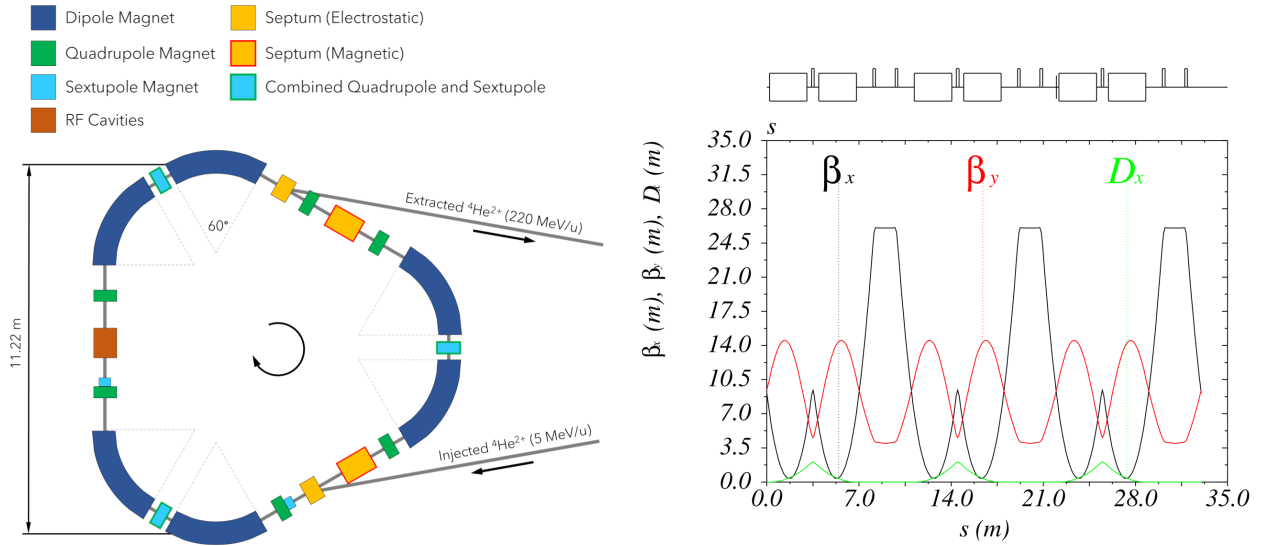
Figure 30: (a) Schematic layout of the NIMMS helium synchrotron, and (b) preliminary optics for the NIMMS synchrotron, calculated in MAD-X. Both figures adapted from Vretenar *et al.* 2023 [7].

$\gtrsim 40$ Gy/s. For a small synchrotron, this implies that the number of ions extracted per spill should be of order $\sim 10^{10}$.

- **Choice of Technologies**

  In keeping with the scope of WP3, the synchrotron should be based entirely in accessible, conventional technologies. For instance, the synchrotron dipoles should be normal conducting, room-temperature magnets rather than high-field superconducting magnets. The machine specifications should not push the limits of conventional technologies beyond what is routinely achieved at other accelerator facilities.

3.1.2 Examples

The Next Ion Medical Machine Study (NIMMS) is an umbrella R&D framework established by CERN to consider designs for next-generation radiotherapy machines. The NIMMS project has already proposed several synchrotron designs relevant to this study, including a superconducting carbon ion machine [59], and a room-temperature helium ion synchrotron [7]. Both designs are intended as the basis for a clinical radiotherapy facility, and therefore accommodate beam energies of several hundred MeV/u and intensities up to 10^{10} ions per cycle.

The NIMMS helium synchrotron (Fig. 30(a)) has a circumference of ~ 33 m, and is designed to deliver helium ions at energies up to 250 MeV/u. The synchrotron lattice is comprised of three identical achromat cells [60], with each cell containing two $60°$ sector dipoles. Each dipole has a bending radius of 2.7 m and a maximum field of 1.65 T, with a small defocusing gradient. A strong quadrupole in centre of each bending section is used to cancel the dispersion along the straights, which accomodate the injection, extraction and RF hardware, respectively. Figure 30(b) shows the beam optics functions around one full turn of the NIMMS helium synchrotron.

The NIMMS designs build on CERN's previous experience with small hadron synchrotrons, such as the ELENA decelerator [61] at the Antiproton Decelerator (AD) facility. ELENA is a small (30.4 m circumference) synchrotron that decelerates antiprotons ($\bar{p}$) from 5.3 MeV to an extraction energy of just 100 keV. While ELENA operates at far lower beam intensities (typically 10^7 $\bar{p}$ per cycle) and repetition rates (approx. 0.01 Hz),

Parameter	Value		
Dipole radius [m]	1.45		
Max. dipole field [T]	1.30		
Max. beam rigidity [T m]	1.89		
Ion species	H^+	$^4He^{2+}$	$^{12}C^{6+}$
Max. beam energy [MeV/u]	80	33.4	33.4
Orbital frequency [MHz]	5.48	3.67	3.67

Table 14: Specifications for the ITRF synchrotron dipole magnets, and the corresponding maximum beam energies for different ion species.

it uses many of the technologies required by the NIMMS synchrotrons. For example, the ELENA RF system is based on a wideband (0.14 – 2 MHz) Finemet cavity, allowing operation over a wide range of energies.

3.2 Synchrotron Design

3.2.1 Machine Layout

The NIMMS helium synchrotron [7] has been used as the basis for the ITRF WP3 synchrotron design, due to its small footprint and large beam intensity. However, the helium synchrotron is still significantly larger than the LhARA FFA and must be scaled down by approximately 30% to fit within the same footprint. Figure 31 shows a schematic layout of the scaled-down WP3 synchrotron, with a circumference of 21.3 m.

Table 14 lists the specifications for the sector dipoles in our scaled version of the NIMMS design. Both the bending radius and field strength of the dipoles have been reduced, such that the maximum beam rigidity is now 1.89 Tm. This allows the ring to accommodate helium and carbon ions up to 33.4 MeV/u, matching the extraction energy of the LhARA FFA [2]. In principle, the dipole magnets can steer proton beams at energies up to 155 MeV. However, we anticipate that the maximum proton energy will be constrained by the bandwidth of the synchrotron RF system. Assuming an RF bandwidth of 1.5 – 5.5 MHz, the synchrotron will accelerate proton beams to a maximum energy of 80 MeV.

3.2.2 Beam Optics

Having established a basic parameter set for the synchrotron, the machine layout was re-optimised to yield a lattice with small beta functions and zero dispersion along the straights. The QF2 quadrupoles (see figure 31) are primarily used to cancel the dispersion introduced by the 60° dipole magnets. In the thin lens approximation, and assuming that the dipoles have no focusing gradient, the focal length of the QF2 quadrupoles is given by

$$f = \frac{\rho\left(1 - \cos\theta\right) + L\sin\theta}{2\sin\theta},\qquad(1)$$

where ρ is the dipole radius, θ is the bending angle and L is the drift length between each dipole and the QF2

quadrupole. Reducing the machine circumference relative to the NIMMS design therefore requires stronger quadrupoles to eliminate the residual dispersion along the straights. The QF2 quadrupole specifications and
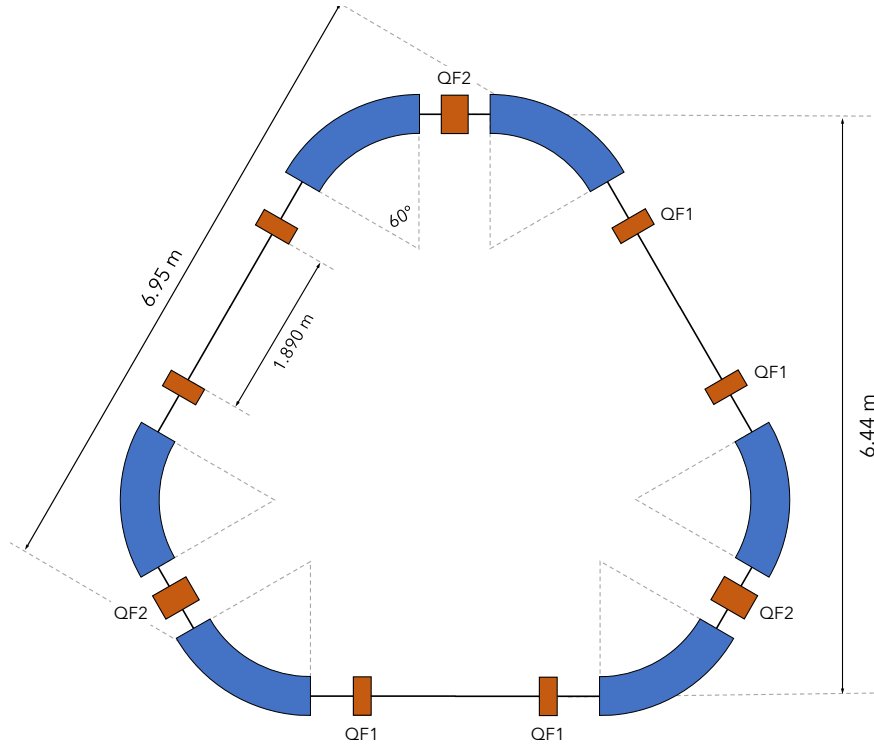
Figure 31: Schematic showing the preliminary layout of the WP3 synchrotron design at the time of writing. Elements are approximately to scale. Dipole (quadrupole) magnets are highlighted in blue (orange).

the layout of the bending sections were therefore optimised to avoid the need for excessively strong focusing gradients.

A python-based linear optics model was developed, and used to identify machine layouts with a wide range of accessible working points. Figure 33 shows the outcome of one such optimisation. Here, the strength of the QF2 quadrupoles has been fixed to cancel the dispersion introduced by the bending sections. The beam optics are therefore determined by the strengths and locations of the QF1 quadrupoles, which are treated as free parameters in the optimisation. Figure 32 shows a schematic layout of the optimised lattice cell.

The beam optics functions were primarily calculated using MAD-X. To enable slow beam extraction using an RF knock-out (RF-KO) scheme, the synchrotron working point must be established close to a third-order betatron resonance. Figure 34 shows the preliminary optics at a working point with $Q_x = 2.33$. By adjusting the strengths of the QF1 quadrupoles, the synchrotron can also be operated at a second working point with $Q_x = 2.67$. The beam optics for this working point are shown in figure 35.

Table 15 summarises the beam optics for both working points. As shown in Figures 34 and 35, the optimised lattice cell produces small beta functions in both planes. The working point with $Q_x = 2.33$ (figure 34) is slightly favourable due to its smaller beta functions and reduced natural chromaticity.

3.3   Injector

3.3.1   Key Parameters

As proposed in both NIMMS designs, we expect that the synchrotron will be filled from a conventional injector that resembles CERN's Linac 4. Several ion sources can be connected to the injector via a magnetic switchyard, allowing a range of ion species to be used interchangeably.
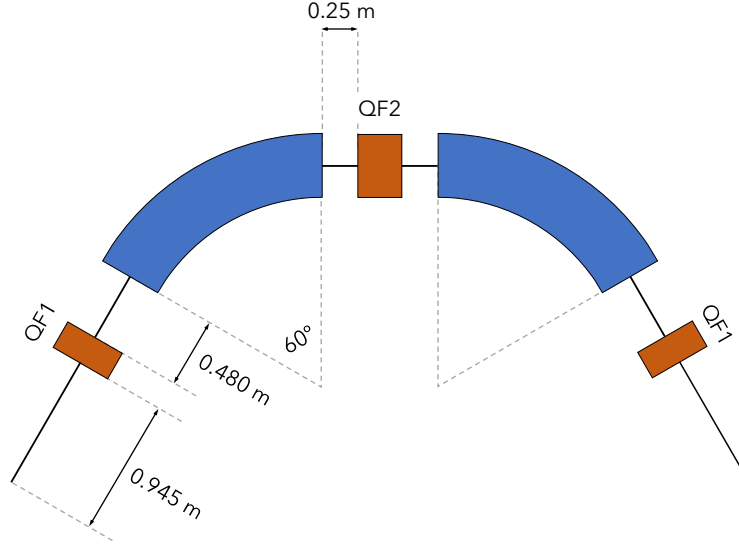
Figure 32: Schematic view showing one of three achromat lattice cells that form the WP3 synchrotron. Elements are approximately to scale and are shaded according to the colour scheme of figure 31.

Parameter	Value	
QF1 Strength [m^{-2}]	3.23	3.72
Betatron Tunes		
Q_x	2.33	2.67
Q_y	0.71	0.52
Optics functions		
Max. β_x [m]	7.20	8.95
Max. β_y [m]	9.92	13.63
Max. D_x [m]	1.98	1.98
Natural Chromaticities		
η_x	-4.36	-6.66
η_y	-5.10	-6.80

Table 15: Beam optics parameters for the synchrotron working points shown in Figures 34 and 35, respectively. Both working points are within the tuning range of the QF1 quadrupoles.

In the NIMMS injector [7], ions are accelerated to a nominal injection energy of 5 MeV/u using a Radio-Frequency Quadrupole (RFQ) followed by a single Drift Tube Linac (DTL) tank. The injection energy of 5 MeV/u was chosen primarily based on the efficiency of typical stripping foils, such as those used to produce carbon ions from ^{12}C^{4+}. To mitigate space charge effects, protons are injected at 10 MeV using a second DTL tank, which can be turned off entirely when working with ions.

For the purposes of this design study, we assume a set of injector parameters based on those of the proposed SEEIST facility [62]. Table 16 lists the expected beam current for protons, helium and carbon ions at injection. Commerical Electron Cyclotron Resonance (ECR) ion sources such as the Pantechnik *Supernanogan* source [63, 64] can provide up to 2 mA of proton current.
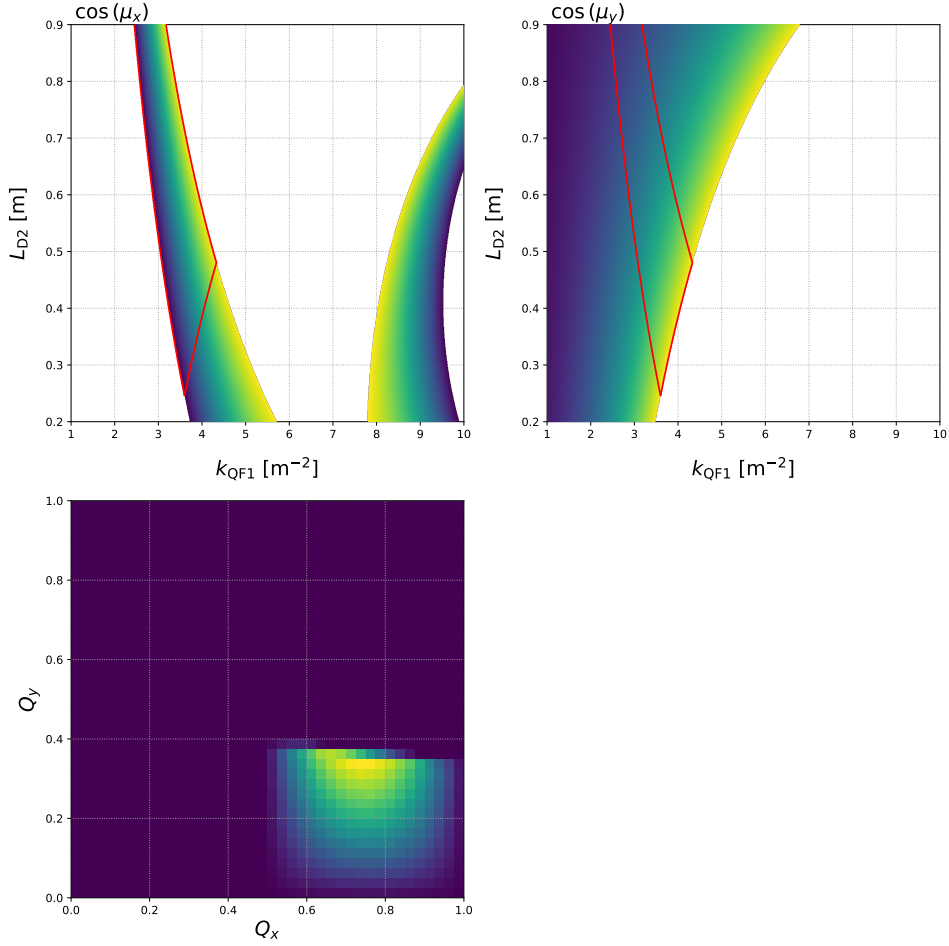
Figure 33: Linear optics calculation showing the tuning parameter space of the ITRF synchrotron lattice. Panel (a) shows the cosine of the horizontal phase advance as a function of the QF1 quadrupole strength k_{QF1} and position L_{D2}, while (b) shows the cosine of the vertical phase advance. Stable lattice configurations are outlined in red. Panel (c) shows the betatron tunes (Q_x, Q_y) for stable lattice configurations.

3.3.2 Muti-Turn Injection

In order to accumulate sufficient ions for FLASH extraction during each synchrotron cycle, we expect to load beam using Multi-Turn (MT) injection. In this scheme, ions are typically injected over $15 - 20$ successive turns. Assuming that the injector emittance is much smaller than the synchrotron acceptance, the phase space of the circulating beam is gradually filled with charge density, as shown in figure 36. The charge distribution is then smoothed out due to phase space filamentation over subsequent turns.

We estimate the stored intensity for each ion species using the parameters in table 16, assuming MT injection over 15 turns with an efficiency of 60 % [65]. The maximum number of circulating ions for both proton and helium is greater than 10^{10}. Only 10^9 carbon ions can be accelerated per synchrotron cycle, due to the lower beam current generated by the carbon ion source.

The tune shift due to the transverse defocusing effect of space charge is largest at injection. In general, a space charge tune shift $|\Delta Q| \leq 0.25$ is considered to be acceptable; larger tune shifts may require a resonance compensation scheme. For each ion species, we estimate the space charge tune shift in the horizontal plane to
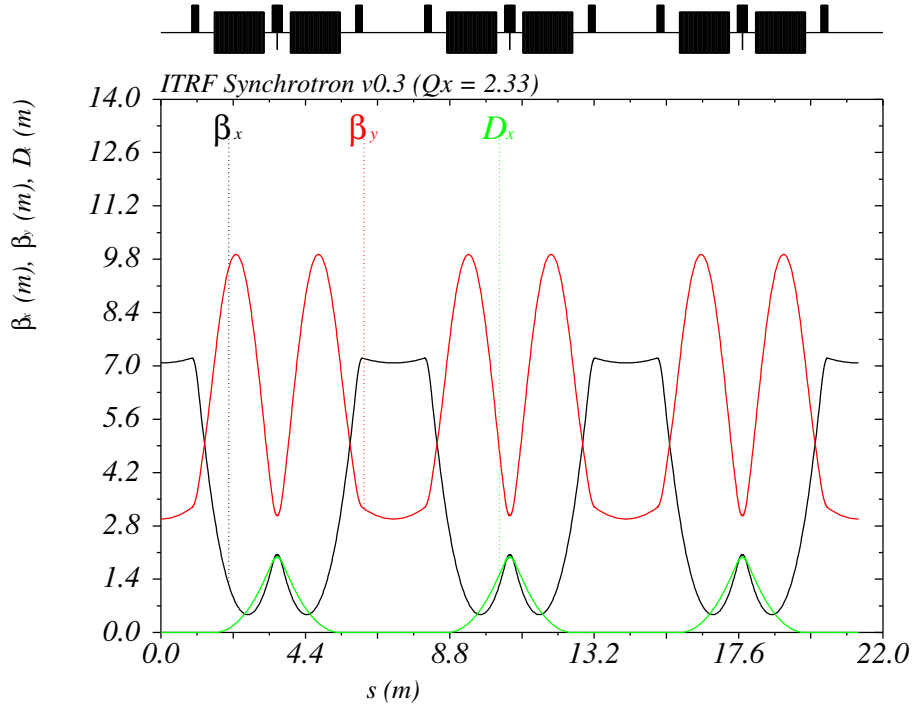
Figure 34: MAD-X calculation showing the preliminary synchrotron optics, with the machine tuned to a working point close to the third-order resonance $Q_x = 2.33$.
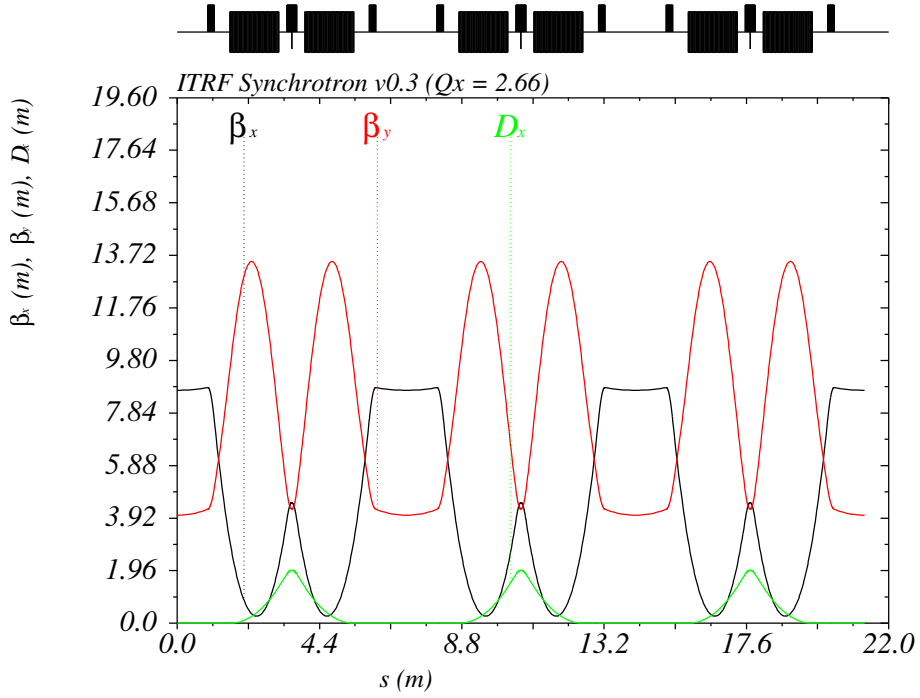

Figure 35: MAD-X calculation showing the preliminary synchrotron optics, with the machine tuned to a working point close to the third-order resonance $Q_x = 2.66$. Note that the scale of the vertical axis is different to that of figure 34.

be

$$\Delta Q_x = -\frac{Z^2 r_p N_0}{2\pi A \beta^2 \gamma^3 \epsilon_x} \left\langle \frac{2}{1 + \sqrt{\epsilon_y \beta_y / \epsilon_x \beta_x}} \right\rangle, \tag{2}$$
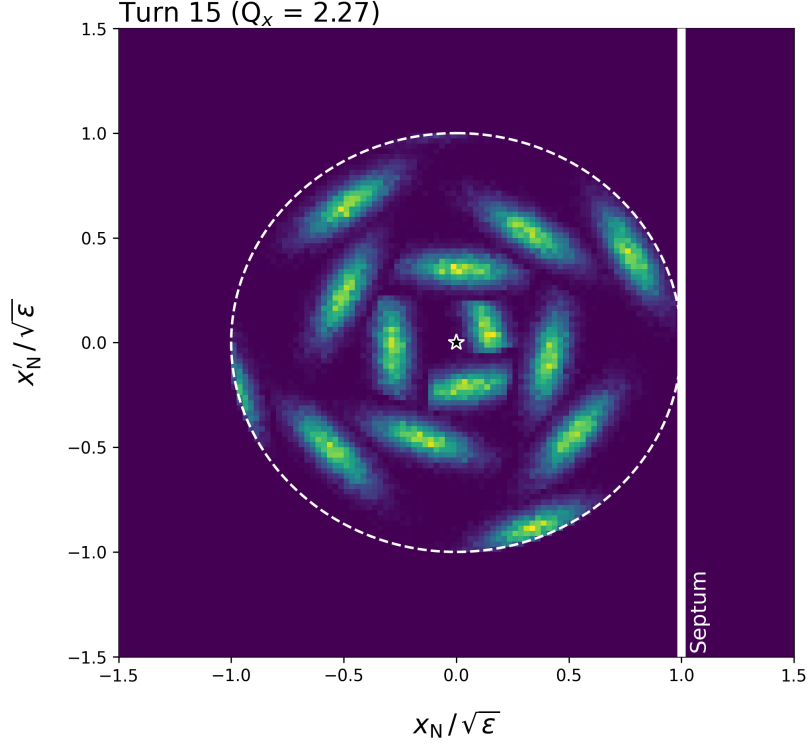
Figure 36: The distribution of charge density in normalised transverse phase space after MT injection. The distribution was calculated using a toy model, assuming a synchrotron tune of $Q_x = 2.27$ and MT injection over 15 turns. The synchrotron acceptance is shown as a dashed white line, and the septum location is indicated as a solid white line.

where N_0 is the number of circulating ions, r_p is the classical proton radius, ϵ_x is the geometric emittance in the horizontal plane, and A and Z are the atomic mass and charge state of the ion, respectively. The relativistic β and γ functions and optical beta functions, $\beta_{x,y}$, are defined as usual. A similar expression can be obtained for the tune shift in the vertical plane.

As shown in table 16, the space-charge tune shift is within an acceptable range for each ion species. Consequently, the number of ions per spill is therefore limited by the injector parameters rather than space charge considerations, in contrast to the original NIMMS designs.

3.4 Beam Extraction

We expect to use an RF knock-out (RF-KO) scheme for slow beam extraction, consistent with the original NIMMS helium synchrotron design. In this scheme, the horizontal tune of the synchrotron is set to a third order resonance (such as $Q_x = 2.33$, as shown in figure 34), which is then driven using sextupole magnets. As particles are driven across the resonance, they are forced to leave the stable region of phase space and are extracted using an electrostatic septum (ES).

Modelling of RF-KO extraction has not yet been performed for the WP3 synchrotron design. However, extensive simulations have been carried out for the NIMMS and PIMMS machines, including those at CNAO and MedAustron [66]. Previous work has shown that RF-KO schemes can be used to extract a uniform spill over a timescale of 0.1 - 1.0 s. For the ITRF synchrotron, an extraction timescale of 100 ms corresponds to around

548000 turns for a proton beam, or 367000 turns for either helium or carbon. Beam extraction on timescales below 100 ms may be possible, but has not yet been explored due to the challenging dosimetry requirements in this regime.

3.5 Extracted Dose Rates

3.5.1 Dose Calculation and Protons

The achievable dose rates from any accelerator source depend not only upon the accelerator source parameters—notably ions per spill, source repetition rate (the latter being here the synchrotron cycling rate), and extracted particle energy—but also upon the field size and depth into which the ions are delivered. To illustrate the likely dose rates that may be obtained, we consider two indicative situations:

- (a) target volume with 3×3 cm field size extending from 0 cm depth to 1 cm depth to encompass a 9 cm^3 volume;
- (b) target volume with 1×1 cm field size extending from 0 cm depth to 1 cm depth to encompass a 1 cm^3 volume.

In both cases we use the ordinary convention of calculating dose rate assuming the irradiated volume is composed of water. For simplicity (since we are in essence concerned with orders of magnitude), we following the method outlined in Owen et al. 2014 [67]. The basis of this method is to note that total deposited energy is merely determined by the number of ions in a spill and by the kinetic energy of each ion. We assume that dose is uniformly deposited over the volume by using a spread-out Bragg peak (SOBP) approach; the extraction energy is therefore adjusted for each depth layer to position a Bragg peak at that depth. There will be some additional dose deposited outside the target volume due to lateral scattering (multiple Couloumb scattering), but given the low ion energies this is a small proportion of the overall energy carried by the incident ions.

Parameter	Values		
	H$^+$	^{4}He^{2+}	^{12}C^{6+}
Linac Current [mA]	2.0	1.0	0.2
Injection Energy [MeV/u]	10.0	5.0	5.0
Orbital Period [MHz]	2.04	1.45	1.45
MT Injection Efficiency [%]		60 %	
Ions After 15 Turns [10^{10}]	5.51	1.94	0.13
Space Charge Tune Shifts			
ΔQ_x	-0.10	-0.01	< 0.01
ΔQ_y	-0.15	-0.02	< 0.01

Table 16: Injector parameters and corresponding stored intensities for different ion species. Injector parameters are based on those of the proposed SEEIST facility [62].

	Ion Species		
	H^+	$^4He^{2+}$	$^{12}C^{6+}$
Extraction Energy [MeV/u]	80	33.4	33.4
Extracted Ions [10^{10}]	5.51	1.94	0.13
Median Ion Energy [MeV/u] (0.5 cm)	21.0	21.8	38.5
Max Ion Energy [MeV/u] (1 cm)	30.9	31.8	56.8*
Target volume (a) 9 cm^3, mid-point range 0.5 cm			
Dose Per Spill [Gy/spill]	20.5	45.2	16.0
Dose Rate During 100 ms Spill [Gy/s]	205	452	160
Average Dose Rate (1 Hz Cycling) [Gy/s]	20.5	45.2	16.0
Target volume (b) 1 cm^3, mid-point range 0.5 cm			
Dose Per Spill [Gy/spill]	185	271	96.2
Dose Rate During 100 ms Spill [Gy/s]	1850	2710	962
Average Dose Rate (1 Hz Cycling) [Gy/s]	185	271	96.2

Table 17: Estimated extracted dose rates for two indicative volumes (a) and (b) as described in the main text, assuming a synchrotron cycling rate of 1 Hz and an extraction duration of 100 ms. Note that the synchrotron option outlined here cannot deliver the carbon ion energy required to reach a depth of 1 cm (starred value in the table).

For protons incident upon either target volume, a 1 cm depth requires 30.9 MeV protons, as estimated using the Bethe-Bloch equation. Here we use a common formula (from the Particle Data Group (PDF) [68]) which is:

$$-\left\langle \frac{dE}{dx} \right\rangle = kz^2 \frac{Z}{A} \frac{1}{\beta^2} \left[\frac{1}{2} \ln \frac{2m_e c^2 \beta^2 \gamma^2 T_{\max}}{I^2} - \beta^2 - \frac{\delta(\beta\gamma)}{2} \right] ; \qquad (3)$$

where Z and A are the atomic number and atomic mass of the absorber, z is the charge of the incident particle, $I \simeq 11.5Z$ eV is the mean ionisation potential, $T_{max} = 2m_e c^2 \beta^2 \gamma^2 / [1 + 2\gamma m_e/M + (m_e/M)^2]$ is the maximum kinetic energy that may be imparted to an electron in a single collision, $k = 4\pi N_A r_e^2 m_e c^2$, and β and γ are the conventional relativistic factors. $\delta(\beta\gamma)$ is a density correction term. We note that the PDG formula overestimates the experimentally achieved range by a few percent [69], but is good enough for the approximate estimates here.

The required energy to place a Bragg peak mid-way through the depth range (at 1.5 cm) is around 21 MeV, and so we use that as an estimate of the average energy deposited by a proton within the target volume; 21 MeV is 3.4 pJ per proton. With an estimated 5.5×10^{10} protons/spill, this is 0.185 J deposited per spill. In a 9 cm³ volume this corresponds to 20.5 Gy dose per spill; if complete beam extraction can be achieved in 100 ms this would be a dose of 205 Gy/s for 100 ms, and a time-averaged dose rate of 20.5 Gy/s over multiple extraction spills at 1 Hz synchrotron cycling rate.

A similar estimate can be made for smaller target volume (b). The same 0.185 J deposited energy within the smaller volume gives nine times the dose, around 185 Gy per spill. 100 ms extraction duration would therefore achieve 185 Gy/s dose rate, and a time-averaged dose rate of 185 Gy/s over multiple spills.

3.5.2 Dose Estimates for Ions

We can make similar estimates of achievable dose rates for heavier ions; here we consider $^4\text{He}^{2+}$ and $^{12}\text{C}^{6+}$ incident again upon the same water volumes. Helium ions of 21.8 MeV/u kinetic energy have a Bragg peak half-way through the two volumes (0.5 cm), and 31.8 MeV/u is needed to reach the deepest (1 cm) depth. Using the same method as for protons but using the lower achievable extracted ion number, the dose per spill is somewhat greater than it is for protons (see table 17). Carbon ion dose rates can be calculated the same way, but it must be noted that the present synchrotron design does not achieve an extracted $^{12}\text{C}^{6+}$ ion energy that can penetrate to 1 cm depth. Despite the lower achievable ion number, the much larger kinetic energy carried by each carbon ion means that the dose rate is comparable to that of protons.

3.6 Conclusions

A preliminary design for a slow-cycling synchrotron has been established as part of ITRF WP3. The synchrotron and its injector have been adapted from designs proposed by the CERN NIMMS project, using established technologies for both the ion sources and accelerator. The synchrotron parameters have been chosen to provide a direct comparison against the LhARA FFA post-acceleration stage, with a similar circumference and final beam energy. The synchrotron optics have been optimised so that a wide range of machine setups are accessible, including at least two working point compatible with RF-KO extraction. We have shown that the expected beam intensities of order 10^{10} ions per cycle are possible, compatible with FLASH dose rates.

References

[1] "LhARA; the Laser-hybrid Accelerator for Radiobiological Applications." `https://ccap.hep.ph.ic.ac.uk/trac/wiki/Research/LhARA`. (Accessed 31-03-2023).

[2] G. Aymar, T. Becker, S. Boogert, M. Borghesi, R. Bingham, C. Brenner, P. N. Burrows, O. C. Ettlinger, T. Dascalu, S. Gibson, T. Greenshaw, S. Gruber, D. Gujral, C. Hardiman, J. Hughes, W. G. Jones, K. Kirkby, A. Kurup, J.-B. Lagrange, K. Long, W. Luk, J. Matheson, P. McKenna, R. McLauchlan, Z. Najmudin, H. T. Lau, J. L. Parsons, J. Pasternak, J. Pozimski, K. Prise, M. Puchalska, P. Ratoff, G. Schettino, W. Shields, S. Smith, J. Thomason, S. Towe, P. Weightman, C. Whyte, and R. Xiao, "LhARA: The Laser-hybrid Accelerator for Radiobiological Applications," *Frontiers in Physics* **8** (2020).

[3] The LhARA consortium, "The Laser-hybrid Accelerator for Radiobiological Applications," Tech. Rep. CCAP-TN-01, The Centre for the Clinical Application of Particles, Imperial College London, 2020. `https://ccap.hep.ph.ic.ac.uk/trac/raw-attachment/wiki/Communication/Notes/CCAP-TN-01.pdf`.

[4] The LhARA collaboration, "The Laser-hybrid Accelerator for Radiobiological Applications: R&D proposal for the preliminary, pre-construction phases," Tech. Rep. CCAP-TN-10, The Centre for the Clinical Application of Particles, Imperial College London, 2022. `https://ccap.hep.ph.ic.ac.uk/trac/raw-attachment/wiki/Communication/Notes/CCAP-TN-10.pdf`.

[5] The LhARA collaboration, "The Laser-hybrid Accelerator for Radiobiological Applications: Scope of work to be carried out under the ITRF Preliminary Activity," Tech. Rep. CCAP-TN-10 Annex, The Centre for the Clinical Application of Particles, Imperial College London, 2022. `https://ccap.hep.ph.ic.ac.uk/trac/raw-attachment/wiki/Communication/Notes/CCAP-TN-10-LhARA-ITRF-proposal-annex.pdf`.

[6] "CERN–UKRI STFC Framework Collaboration Agreement KN 5444/ATS concerning the Development of Next Generation Ion Beam Acceleration Technologies for Cancer Treatment and its Associated Research," 2022.

[7] M. Vretenar, M. E. Angolettai, G. Bisoffi, J. Borburgh, L. Bottura, K. Paļskis, R. Taylor, G. Tranquille, E. Benedetto, and M. Sapinski, "A Compact Synchrotron for Advanced Cancer Therapy with Helium and Proton Beams," *Journal of Physics: Conference Series* **2420** (jan, 2023) 012103.

[8] "ITRF document naming convention." 1272-pa1-pm-rpt-0002-v1.0-ITRF-document-naming Ion Therapy Research Facility - rpt - Reports - All Documents (sharepoint.com).

[9] "ITRF SharePoint site." `https://stfc365.sharepoint.com/sites/ITRF`.

[10] "ITRF project roles and responsibility, 1272-pa1-pm-pmp-0004-v1.5-roles-governance." `https://stfc365.sharepoint.com/sites/ITRF/` Ion Therapy Research Facility - pmp - Project Management Plan - All Documents (sharepoint.com).

[11] "ISO9001 Quality Management ." `https://www.iso.org/iso-9001-quality-management.html`.

[12] "BSI ISO 9001 Certification." `https://www.bsigroup.com/en-GB/iso-9001-quality-management/Certification-for-ISO-9001/`.

[13] "Business Case, 1272-pa1-pm-rpt-0003-v1.0-business-case."
`https://stfc365.sharepoint.com/sites/ITRF/`" Ion Therapy Research Facility - rpt -
Reports - All Documents (sharepoint.com).

[14] "Project Management Plan, 1272-pa1-pm-pmp-0001-v9.0-ITRF-2023-03-09."
`https://stfc365.sharepoint.com/sites/ITRF/` Ion Therapy Research Facility - pmp -
Project Management Plan - All Documents (sharepoint.com).

[15] **LhARA** Collaboration, "The LhARA initiative," 2021.
`https://ccap.hep.ph.ic.ac.uk/trac/raw-attachment/wiki/Research/`
`DesignStudy/2021-10-02-LhARA-Brief-Final.pdf`.

[16] "Infrastructure Fund projects." https://www.ukri.org/what-we-offer/creating-world-class-research-and-
innovation-infrastructure/funded-infrastructure-projects/, July, 2022. Accessed: 2023-03-21.

[17] **LhARA** Collaboration, "LhARA Project Management Board pages." `https://ccap.hep.ph.ic.`
`ac.uk/trac/wiki/Research/LhARA/Governance/ProjectManagementBoard`, 2023.
Accessed: 2023-03-21.

[18] **LhARA** Collaboration, "Laser-driven proton and ion source." `https:`
`//ccap.hep.ph.ic.ac.uk/trac/wiki/Research/LhARA/LaserDrivenSource`, 2023.
Accessed: 2023-03-21.

[19] **LhARA** Collaboration, "Gabor Lens."
`https://ccap.hep.ph.ic.ac.uk/trac/wiki/Research/LhARA/GaborLens`, 2023.
Accessed: 2023-03-21.

[20] **LhARA** Collaboration, "Ionacoustic dose mapping."
`https://ccap.hep.ph.ic.ac.uk/trac/wiki/Research/LhARA/IonAcoustic`, 2023.
Accessed: 2023-03-21.

[21] **LhARA** Collaboration, "End station R&D and vertical beam line development."
`https://ccap.hep.ph.ic.ac.uk/trac/wiki/Research/LhARA/EndStation`, 2023.
Accessed: 2023-03-21.

[22] **LhARA** Collaboration, "Accelerator design and facility integration." `https:`
`//ccap.hep.ph.ic.ac.uk/trac/wiki/Research/LhARA/DesignAndIntegration`,
2023. Accessed: 2023-03-21.

[23] **LhARA** Collaboration, "LhARA Executive Board." `https://ccap.hep.ph.ic.ac.uk/trac/`
`wiki/Research/LhARA/Governance/ExecutiveBoard`, 2023. Accessed: 2023-03-21.

[24] **LhARA** Collaboration, "Review of the collaboration's "R&D proposal for the preliminary and
pre-construction phases"." `https://ccap.hep.ph.ic.ac.uk/trac/wiki/Research/`
`LhARA/Governance/ExecutiveBoard/Reviews/AugOct22`, 2023. Accessed: 2023-03-21.

[25] LhARA PMB, "Review of the collaboration's "R&D proposal for the preliminary and pre-construction
phases" Response to feedback," Tech. Rep. LhARA-Gov-PMB-2022-02, The Centre for the Clinical
Application of Particles, Imperial College London, 2023.
`https://ccap.hep.ph.ic.ac.uk/trac/raw-attachment/wiki/Research/LhARA/`
`Documentation/TN/Governance/LhARA-Gov-PMB-2022-02.pdf`.

[26] M. Lamont et al., "Review of the collaboration's "R&D proposal for the preliminary and pre-construction phases"; Feedback," Tech. Rep. LhARA-Gov-Rev-2022-01, The Centre for the Clinical Application of Particles, Imperial College London, 2022. `https://ccap.hep.ph.ic.ac.uk/trac/raw-attachment/wiki/Research/LhARA/Documentation/TN/Governance/LhARA-Gov-Rev-2022-01.pdf`.

[27] **LhARA** Collaboration, "NOVEL END-STATION DEVELOPMENT: CONSULTATION 1." `https://indico.stfc.ac.uk/event/668/`, 2022. Accessed: 2023-03-21.

[28] **LhARA** Collaboration, "LhARA Collaboration Meeting." `https://indico.stfc.ac.uk/event/685/`, 2023. Accessed: 2023-03-21.

[29] D. Mariscal, B. Djordjevíc, E. Grace, R. Hollinger, T. Ma, G. Scott, H. Song, R. Simpson, J. Rocca, and S. Wang, "Design of flexible proton beam imaging energy spectrometers (PROBIES)," *Plasma Physics and Controlled Fusion* **63** (2021), no. 11, 114003.

[30] "VSim (Tech-X)." `https://txcorp.com/vsim/`.

[31] J.-L. Vay, A. Almgren, J. Bell, L. Ge, D. Grote, M. Hogan, O. Kononenko, R. Lehe, A. Myers, C. Ng, J. Park, R. Ryne, O. Shapoval, M. Thévenet, and W. Zhang, "Warp-X: A new exascale computing platform for beam–plasma simulations," *Nuclear Instruments and Methods in Physics Research Section A: Accelerators, Spectrometers, Detectors and Associated Equipment* **909** (2018) 476–479. 3rd European Advanced Accelerator Concepts workshop (EAAC2017).

[32] "WarpX." `https://github.com/ECP-WarpX/WarpX`.

[33] "Geant4." `https://geant4.web.cern.ch/`.

[34] "k-Wave." `http://www.k-wave.org/`.

[35] M. Maxouti, "Development of an ion-acoustic dose-deposition mapping system for LhARA," Tech. Rep. CCAP-TN-INST-04, The Centre for the Clinical Application of Particles, Imperial College London, 2022. `https://ccap.hep.ph.ic.ac.uk/trac/raw-attachment/wiki/Communication/Notes/CCAP-TN-INST-04.pdf`.

[36] A. MacIntosh-LaRocque, "Investigating Detector Specifications for Ionacoustic Imaging of Proton Beams," Tech. Rep. CCAP-TN-INST-05, The Centre for the Clinical Application of Particles, Imperial College London, 2022. `https://ccap.hep.ph.ic.ac.uk/trac/raw-attachment/wiki/Communication/Notes/CCAP-TN-INST-05.pdf`.

[37] "Ion acoustic dose mapping." `https://ccap.hep.ph.ic.ac.uk/trac/wiki/Research/LhARA/IonAcoustic`. (Accessed 31-03-2023).

[38] T. Bortfeld, "An analytical approximation of the Bragg curve for therapeutic proton beams," *Medical Physics* **24** (1997), no. 12, 2024–2033, `https://aapm.onlinelibrary.wiley.com/doi/pdf/10.1118/1.598116`.

[39] "EUPRAXIA-DN." `https://www.eupraxia-dn.org/`.

[40] "NOVEL END-STATION DEVELOPMENT: CONSULTATION 1." `https://indico.stfc.ac.uk/event/668/`.

[41] The LhARA collaboration, "Baseline for the LhARA design update," Tech. Rep. CCAP-TN-11, The Centre for the Clinical Application of Particles, Imperial College London, 2022. `https://ccap.hep.ph.ic.ac.uk/trac/raw-attachment/wiki/Communication/Notes/CCAP-TN-11-LhARA-Design-Baseline.pdf`.

[42] International Organization for Standardization, "Cleanrooms and associated controlled environments — Part 1: Classification of air cleanliness by particle concentration," Tech. Rep. ISO 14644-1:2015, International Organization for Standardization, 2015. `https://www.iso.org/standard/53394.html`.

[43] F. S. Englbrecht, A. Döpp, J. Hartmann, F. H. Lindner, M. L. Groß, H.-F. Wirth, P. G. Thirolf, S. Karsch, J. Schreiber, K. Parodi, and G. Dedes, "Radiation protection modelling for 2.5 Petawatt-laser production of ultrashort x-ray, proton and ion bunches: Monte Carlo model of the Munich CALA facility," *Journal of Radiological Protection* **40** (sep, 2020) 1048.

[44] Forster Ingenieurgesellschaft, "Forster Ingenieurgesellschaft - References." `https://forster-bau.de/en/references/`. Accessed: 2023-04-04.

[45] Health and Safety Executive (HSE), *Working with ionising radiation. Ionising Radiations Regulations 2017. Approved Code of Practice and guidance.* TSO (The Stationery Office), 2018.

[46] International Electrotechnical Commission, *Functional safety of electrical/electronic/programmable electronic safety-related systems.* International Electrotechnical Commission, 2010.

[47] Health and Safety Executive (HSE), *Working with ionising radiation. Ionising Radiations Regulations 1999. Approved Code of Practice and guidance.* TSO (The Stationery Office), 2000.

[48] The LhARA Collaboration, "LhARA draft schematic diagram." Document: 1272-pa1-pm-sch-0001-v1.1-LhARA schematic, 2023.

[49] The LhARA Collaboration, "LhARA draft device naming convention proposal." Document: 1272-pa1-ctrl-rpt-0001-v0.5-LhARA-device-naming, 2023.

[50] The EPICS Collaboration, "Experimental Physics and Industrial Control System." `https://epics-controls.org/`.

[51] "Methodical Accelerator Design X." `http://madx.web.cern.ch/madx`.

[52] Y. Chao, "BeamOptics: A symbolic platform for modeling and the solution of beam optics system," *tech. rep.* (2000).

[53] PulsarPhysics, "General Particle Tracer,". `http://www.pulsar.nl/gpt/index.html`.

[54] L. N. et al, "BDSIM: An accelerator tracking code with particle-matter interactions," *Computer Physics Communications* (2020) 107200.

[55] J. D. *et al.*, "Smilei : A collaborative, open-source, multi-purpose particle-in-cell code for plasma simulation," *Computer Physics Communications* **222** (2018) 351–373.

[56] H. T. L. *et. al.*, "Beam Tracking Simulations for Stage 1 of the Laser-hybrid Accelerator for Radiobiological Applications (LhARA)," *Proc. 12th Int. Particle Accelerator Conf. (IPAC'21)* **WEPAB139** (2021) 2939–2942.

[57] R. A. Fonseca, L. O. Silva, F. S. Tsung, V. K. Decyk, W. Lu, C. Ren, W. B. Mori, S. Deng, S. Lee, T. Katsouleas, and J. C. Adam, "OSIRIS: A Three-Dimensional, Fully Relativistic Particle in Cell Code for Modeling Plasma Based Accelerators," in *Computational Science — ICCS 2002*, pp. 342–351. 2002.

[58] K. J. Kirkby, N. F. Kirkby, N. G. Burnet, H. Owen, R. I. Mackay, A. Crellin, and S. Green, "Heavy Charged Particle Beam Therapy and Related New Radiotherapy Technologies: The Clinical Potential, Physics and Technical Developments Required to Deliver Benefit for Patients with Cancer," *The British Journal of Radiology* **93** (2020), no. 1116, 20200247, `https://doi.org/10.1259/bjr.20200247`. PMID: 33021102.

[59] H. Norman, R. Appleby, E. Benedetto, M. Karppinen, H. Owen, and S. Sheehy, "Performance Study of the NIMMS Superconducting Compact Synchrotron for Ion Therapy with Strongly Curved Magnets," *JACoW IPAC* **2022** (2022) 3014–3017.

[60] X. Zhang, "Lattice Design of a Carbon-Ion Synchrotron based on Double-Bend Achromat Lens," 2020.

[61] V. Chohan *et al.*, *Extra Low ENergy Antiproton (ELENA) ring and its Transfer Lines: Design Report*. CERN Yellow Reports: Monographs. CERN, Geneva, 2014.

[62] U Amaldi and J. Balosso and M Dosanjh and J Overgaard and S Rossi and M Scholz and B Singers Sorensen, *A Facility for Tumour Therapy and Biomedical Research in South-Eastern Europe*. CERN Yellow Reports: Monographs. CERN, Geneva, 2019.

[63] "PANTECHNIK ECR Ion Sources." `https://www.pantechnik.com/ecr-ion-sources`. (Accessed 17-03-2023).

[64] M. Muramatsu and A. Kitagawa, "A Review of Ion Sources for Medical Accelerators," *Review of Scientific Instruments* **83** (2012), no. 2, 02B909, `https://doi.org/10.1063/1.3671744`.

[65] E. Benedetto, "Carbon Ion Compact Medical Synchrotron: Key Parameters, CERN-ACC-NOTE-2022-0017, NIMMS-Note-008,".

[66] R. Taylor, E. Benedetto, M. Sapinski, and J. Pasternak, "Slow Extraction Modelling for NIMMS Hadron Therapy Synchrotrons," *Journal of Physics: Conference Series* **2420** (jan, 2023) 012101.

[67] H. Owen, R. MacKay, K. Peach, and S. Smith, "Hadron Accelerators for Radiotherapy," *Contemporary Physics* **55** (2014), no. 2, 55–74, `https://doi.org/10.1080/00107514.2014.891313`.

[68] J. Beringer *et al.*, "Review of Particle Physics," *Physical Review D* **86** (2012), no. 11, 010001.

[69] M. K. Hamad, "Bragg-curve simulation of carbon-ion beams for particle-therapy applications: A study with the GEANT4 toolkit," *Nuclear Engineering and Technology* **53** (2021), no. 8, 2767–2773.